Jorma Joutsensaari

Aerosol synthesis of nanostructured, ultrafine fullerene particles

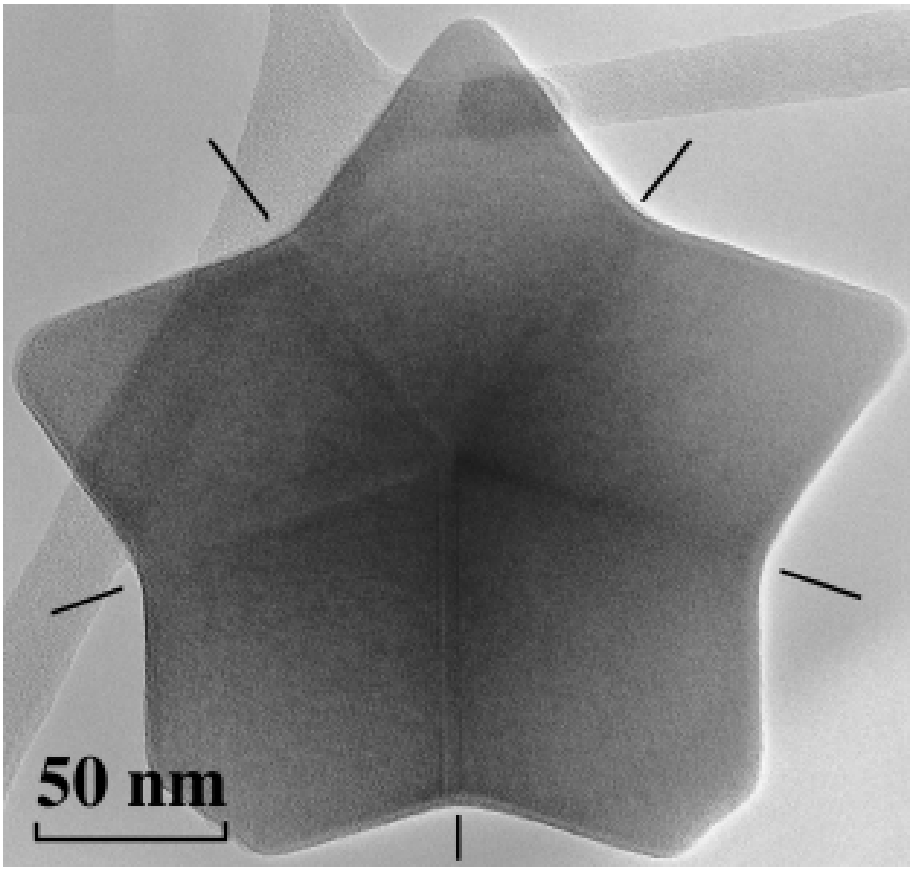

TECHNICAL RESEARCH CENTRE OF FINLAND ESPOO 1999

VTT PUBLICATIONS 400

Aerosol synthesis of nanostructured, ultrafine fullerene particles

Jorma Joutsensaari

VTT Chemical Technology

Thesis for the degree of Doctor of Technology to be presented with due permission for public examination and criticism in Auditorium Rg202 at Tampere University of Technology on the 17th of December, 1999, at 12 o'clock noon.

TECHNICAL RESEARCH CENTRE OF FINLAND
ESPOO 1999

ISBN 951–38–5545–7 (soft back ed.)
ISSN 1235–0621 (soft back ed.)

ISBN 951–38–5548–1 (URL: http://www.inf.vtt.fi/pdf/)
ISSN 1455–0849 (URL: http://www.inf.vtt.fi/pdf/)

JULKAISIJA – UTGIVARE – PUBLISHER

Valtion teknillinen tutkimuskeskus (VTT), Vuorimiehentie 5, PL 2000, 02044 VTT
puh. vaihde (09) 4561, faksi (09) 456 4374

Statens tekniska forskningscentral (VTT), Bergsmansvägen 5, PB 2000, 02044 VTT
tel. växel (09) 4561, fax (09) 456 4374

Technical Research Centre of Finland (VTT), Vuorimiehentie 5, P.O.Box 2000, FIN–02044 VTT, Finland
phone internat. + 358 9 4561, fax + 358 9 456 4374

VTT Kemiantekniikka, Prosessitekniikka, Biologinkuja 7, PL 1401, 02044 VTT
puh. vaihde (09) 4561, faksi (09) 456 7021

VTT Kemiteknik, Processteknik, Biologgränden 7, PB 1401, 02044 VTT
tel. växel (09) 4561, fax (09) 456 7021,

VTT Chemical Technology, Process Technology, Biologinkuja 7, P.O.Box 1401, FIN–02044 VTT, Finland
phone internat. + 358 9 4561, fax + 358 9 456 7021

Cover picture:
A TEM image of a multiply-twinned particle (courtesy of D. Bernaerts and G. Van Tendeloo, EMAT, University of Antwerp, Belgium).

Technical editing Maini Manninen

Libella Painopalvelu Oy, Espoo 1999

Joutsensaari, Jorma. Aerosol synthesis of nanostructured, ultrafine fullerene particles. Espoo 1999. Technical Research Centre of Finland, VTT Publications 400. 64 p. + app. 101 p.

Keywords aerosols, synthesis, nanostructured materials, particles, fullerenes, vapor condensation, droplet drying, crystallization, transmission electron microscopy, morphology

Abstract

Aerosol synthesis methods for the production of nanostructured fullerene particles have been developed. The nanostructured, ultrafine fullerene particles were produced by vapor condensation and aerosol droplet drying and crystallization methods in tubular laminar flow reactors. The formation mechanisms were studied by measuring particle-size distributions is the gas phase. High-resolution scanning and transmission electron microscopy methods were used to observe particle morphology and crystal structure, and to study the crystallization mechanisms of the fullerene particles. The production conditions of fullerene particles during synthesis, i.e. gas temperature and flow profiles in the reactor, were evaluated using computational fluid dynamics calculations. In order to study the role of fullerene vapor during crystallization, fullerene particle evaporation dynamics in the laminar flow was modeled using aerosol particle evaporation theory. In addition, a high-performance liquid chromatography method was utilized to study whether it was possible to separate different fullerenes during aerosol processes.

The study demonstrated that ultrafine (30–60 nm) fullerene particles can be generated by vapor condensation in a continuous-flow reactor. The size of the fullerene particles can be controlled by varying the reactor temperature. The ultrafine particles are spherical, solid and polycrystalline at processing temperatures of 500 °C and above.

The larger fullerene particles with sizes around 100 nm were produced via an aerosol droplet drying method, starting from fullerene-toluene solution droplets. The particles are roughly spherical with pores and voids, and are nanocrystalline when produced at low reactor operating temperatures (20–200 °C). At higher temperatures of up to 400 °C, the particles are denser and mostly polycrystalline. The crystallinity of a fullerene particle can be controlled by changing the reactor operating temperature during the aerosol droplet drying synthesis.

Fullerene particles with clear faceted shapes were observed at processing temperatures of 500 °C and above. The most common shapes along perfectly faceted particles were hexagonal plate-like, decahedral and icosahedral shapes. The high-resolution electron microscopy shows that the plate-like particles are lamellar twinned and the decahedral and icosahedral particles are multiply twinned. The lamellar-twinned particles probably grow rapidly on the side-faces in the direction parallel to the twins by a re-entrant corner growth mechanism. No uniform mechanism was found for the formation of multiply-twinned particles. They probably grow layer-by-layer around the exiting decahedral and icosahedral nuclei. Furthermore, the multiply-twinned particles can be formed during grain growth from polycrystalline particles. The growth of the particles with a well-defined crystal habit is often promoted by defects, such as twins and stacking faults.

The vaporization of fullerene particles in the heated zone of the reactor plays an important role during the formation and growth of particles with a clearly faceted shape. At 500 °C, the growth of the particles mainly occurs in the heated zone of the reactor by partial evaporation and subsequent condensation back onto the particles with defects. At 600 °C, the particles have a less distinct crystal habit due to the almost complete vaporization of the particles in the heated zone. Subsequently, fullerene vapor condenses onto the surfaces of the residual particles. In addition at 500–600 °C, new ultrafine particles are formed via homogeneous nucleation and condensation from fullerene vapor at the reactor outlet where the carrier gas cools down.

Computational fluid dynamics calculations show that with a careful reactor design, uniform conditions with respect to temperature and flow profiles, as well as residence times in the heated zone, can be achieved. Particles with relatively homogeneous crystallinity and morphology can be produced in the uniform reactor conditions. Experiments show that almost all of the particles are hexagonal platelets produced in particular processing conditions at 500 °C.

The high-performance liquid-chromatography results indicate that only minor fractionation occurs during the synthesis of mixed fullerene particles, due to the small difference of partial vapor pressures. Furthermore, C_{60} and C_{70} molecules are fully miscible in the crystals of the particles. It is difficult to separate different fullerenes by aerosol droplet drying, vaporization of fullerenes and subsequent vapor condensation, when starting from C_{60}–C_{70} solution droplets.

Preface

This work has been carried out at the Aerosol Technology Group of VTT Chemical Technology. I wish to express my gratitude to Dr. Esko Kauppinen, the head of the group, for supervising and guiding my thesis work, and providing an excellent research environment for this work. I am also grateful to Prof. Gunnar Graeffe and Prof. Rolf Hernberg for their encouragement and supervision that helped me to complete this thesis.

I am also grateful to all my co-authors and colleagues involved in this work for their valuable contribution. I would especially like to thank Prof. Toivo Kodas and Prof. Gustaaf Van Tendeloo for their helpful collaboration and their guidance in materials science and electron microscopy. Furthermore, I wish to thank Mr. Petri Ahonen, Dr. Dirk Bernaerts, Dr. Abhijit Gurav, Mr. Bart Pauwels and Dr. An Van Cleempoel for their successful co-operation with me in particle synthesis and characterization, and Mr. Raoul Järvinen for his help in carrying out the experiments. I am also grateful to Dr. Kari Lehtinen for his valuable comments and suggestions regarding the writing of the thesis.

This research was funded by the Technology Development Center (Tekes), VTT Chemical Technology, Ventipress Ltd. and the European Science Foundation (ESF). The financial support is gratefully acknowledged.

I wish to thank all my colleagues in the Aerosol Technology Group for a pleasant working atmosphere and for their sincere friendship.

Finally, I thank Terhi, Jussi and Jyri for their understanding and support throughout this work, especially during those many days when I was far away from home, in Espoo and Antwerp.

Kuopio, November 1999

Jorma Joutsensaari

List of publications

This thesis is based on the following publications. In the text they are referred to by Roman numerals.

I Gurav, A. S., Kodas, T. T., Wang, L.-M., Kauppinen, E. I. and Joutsensaari, J. 1994. Generation of nanometer-size fullerene particles via vapor condensation. Chemical Physics Letters, Vol. 218, p. 304–308.

II Joutsensaari, J., Ahonen, P., Tapper, U., Kauppinen, E. I., Laurila, J. and Kuokkala, V.-T. 1996. Generation of nanophase fullerene particles via aerosol routes. Synthetic Metals, Vol. 77, p. 85–88.

III Van Cleempoel, A., Joutsensaari, J., Kauppinen, E., Gijbels, R. and Claeys, M. 1998. Aerosol synthesis and characterization of ultrafine fullerene particles. Fullerene Science and Technology, Vol. 6, p. 599–627.

IV Joutsensaari, J., Kauppinen, E. I., Bernaerts, D. and Van Tendeloo, G. 1998. Crystal growth studies during aerosol synthesis of nanostructured fullerene particles. Materials Research Society Symposium Proceedings, Vol. 520, p. 63–68.

V Pauwels, B., Bernaerts, D., Amelinckx, S., Van Tendeloo, G., Joutsensaari, J. and Kauppinen, E. I. 1999. Multiply twinned C_{60} and C_{70} nanoparticles. Journal of Crystal Growth, Vol. 200, p. 126–136.

VI Joutsensaari, J., Ahonen, P. P., Kauppinen, E. I., Brown, D. P., Lehtinen, K. E. J., Jokiniemi, J. K., Pauwels, B. and Van Tendeloo, G. 1999. Aerosol synthesis of faceted fullerene nanocrystals in controlled flow reactor conditions. Submitted to Journal of Nanoparticle Research.

Author's contribution

The research reported in this thesis was mainly carried out at the Aerosol Technology Group of VTT Chemical Technology, Finland during 1993–1999. Paper I deals with a vapor condensation generation of nanometer-sized fullerene particles, and the experiments were carried out at the University of New Mexico, USA. The particle production experiments of this paper were mainly carried out by Dr. A. Gurav and the author under the supervision of Prof. T. T. Kodas and Dr. E. I. Kauppinen. In addition, the aerosol measurements, data analysis and interpretation were performed by the author.

Papers II–VI are based on the author's experimental work to produce fullerene particles by an aerosol droplet drying and crystallization method. Dr. E. I. Kauppinen supervised the work. The experiments were carried out with the help of Dr. A. Van Cleempoel and Mr. P. Ahonen. Aerosol measurements, described in Papers II–VI, and the scanning electron microscopy analysis described in Papers III–VI were performed and the results were interpreted by the author. The high-performance liquid chromatography analyses of Paper III were carried out by Dr. A. Van Cleempoel under supervision of Prof. R. Gijbels and Prof. M. Claeys. The transmission electron microscopy analyses (TEM) were carried out by Mr. J. Laurila for Paper II, and by Dr. D. Bernaerts, Mr. B. Pauwels and Prof. G. Van Tendeloo for Papers IV–VI. The author assisted in the data interpretation of the TEM results. The evaporation calculations of Paper VI were done by the author with the help of Dr. K. E. Lehtinen. The computational fluid dynamics calculations of Paper VI were performed by Dr. D. P. Brown. The results of the calculations were interpreted mainly by the author. The author wrote Papers II, IV and VI and assisted in writing Papers I, III and V.

Contents

Appendices of this publication are not included in the PDF version. Please order the printed version to get the complete publication (http://www.inf.vtt.fi/pdf/publications/1999/)

List of acronyms and symbols

C_{60}	buckminsterfullerene, fullerene molecule with 60 carbon atoms
C_{70}	fullerene molecule with 70 carbon atoms
CFD	computational fluid dynamics
DMA	differential mobility analyzer
ED	electron diffraction
fcc	face-centered cubic structure
hcp	hexagonal close-packed structure
HPLC	high performance liquid chromatography
HREM	high resolution electron microscopy
LPI	low pressure impactor
MF	mixed fullerenes
MFE	mixed fullerene extract
MTP	multiply twinned particle
PBC	periodic bond chain theory
SEM	scanning electron microscopy
T	temperature
TEM	transmission electron microscopy
δ	height of the elementary growth layer

1. Introduction

The discovery of fullerenes (C_{60}, C_{70}, etc.) has caused the development of new areas of chemistry and physics regarding carbon-based materials. Fullerenes and related materials are exciting from both fundamental and technological viewpoints because of interesting properties such as superconductivity, ferromagnetism and nonlinear optical characteristics. Possible applications of fullerenes and fullerene based materials include superconducting and nanoscale devices, catalysts, optical limiters, carbon composites and molecular sieves. Furthermore, fullerene molecules are interesting due to their unique structure. The C_{60} fullerene, which is a closed cage of 60 carbon atoms with a shape of a truncated icosahedron (a soccer ball), is perhaps the most symmetric molecule (Dresselhaus et al., 1996), and is probably the perfect nanoscale structural unit (Ball and Garwin, 1992).

The gas-phase synthesis of fullerenes and growth of large crystals is well established. However, when developing new applications for fullerene-based nanomaterials, there is a considerable need to develop controlled processing routes that begin with purified fullerenes and produce fullerene-based materials in different particulate and nanostructured forms. Nanostructured materials and nanometer-size particles with a grain and/or particle size in the nanometer size region have a large volume fraction of atoms at their surfaces and grain boundaries. As a result of such a microstructure, they have interesting and possibly useful mechanical, optical, electrical, magnetic and catalytic properties (Gleiter, 1992; Ichinose et al., 1992; Edelstein and Cammarata, 1996).

This overview focuses mainly on aerosol synthesis of fullerene particles in nanostructured, ultrafine forms. In general, high-purity powders with controlled particle size and crystallinity can be produced by aerosol processing methods. Furthermore, aerosol methods can be used to produce materials that contain or are composed of particles or grains in the nanometer size range. Therefore, aerosol routes are promising methods for the production of nanostructured materials (Pratsinis and Kodas, 1993; Kodas and Hampden-Smith, 1999).

The primary objectives of the thesis are to develop aerosol processing routes for nanostructured fullerene particles and to understand their formation and crystallization mechanisms. The particle formation and crystallization mechanisms need to be understood in order to control fullerene particle size and

crystallinity during aerosol synthesis. The work of this thesis was initiated to demonstrate that ultrafine fullerene particles can be generated via a vapor condensation method in a continuous flow reactor system at ambient pressure (Paper I). Later, the work was continued to produce nanostructured fullerene particles by a aerosol droplet drying and crystallization method. In that system, the particle formation mechanisms and crystallization were further studied (Papers II and III). In addition, the possibility of separating different fullerenes when particles are produced from droplets of C_{60} and C_{70} in toluene (Paper III) was studied. Recently, the work has concentrated more on the crystal growth mechanisms of fullerene particles with a well-defined crystal habit (Papers IV–VI). Furthermore, the reactor constructions were improved to achieve uniform conditions (flow and temperature profiles, residence times) for homogeneous particle production (Paper VI). The results of the above-mentioned studies, described in Papers I–VI, are summarized and discussed in this overview.

This thesis is organized as follows. Firstly, a short literature review on fullerenes, materials processing, and the production of fullerene particles introduces the background to this work. Secondly, the production and characterization methods are described in Chapter 3. The fullerene particles were produced in laminar flow reactors and characterized by aerosol measurement techniques, electron microscopy and high-performance liquid chromatography. In addition, computational fluid dynamics (CFD) calculations were performed to examine reactor conditions and, finally, evaporation calculations were carried out to estimate the vaporization of fullerene particles during the synthesis.

The main results of Papers I–VI are discussed in detail in the following chapters. The experiments show that it is possible to produce particles with controlled crystallinity and morphology. Fullerene particles are fine-grained, nanocrystalline at low processing temperatures and they are polycrystalline or single crystals at higher temperatures. Many of the crystalline particles are perfectly faceted. Their shape is typically hexagonal plate-like, decahedral or icosahedral. The plate-like particles are lamellar twinned and the decahedral and icosahedral particles are multiply twinned. The formation and crystallization mechanisms of fullerene particles during aerosol synthesis are discussed. Finally, this work is brought to a conclusion and some recommendations for future studies are discussed.

2. Literature review

This literature review briefly introduces fullerenes, nanostructured materials and aerosol methods for particle production. The synthesis of fullerene based materials in particulate and nanostructured forms is discussed in more detail.

2.1 Fullerenes

The discovery of fullerenes and some of the solid state properties of fullerenes are briefly introduced in this chapter. In addition, the synthesis of the different forms of solid fullerene materials is described. Finally, some possible applications of fullerene nanomaterials are introduced.

2.1.1 Background of fullerenes

Fullerenes (C_{60}, C_{70}, etc.) are a novel family of carbon allotropes. The best known fullerene molecule is the buckminsterfullerene, C_{60}, which has 60 carbon atoms forming a truncated icosahedral structure with twelve pentagonal and twenty hexagonal rings. The structure is essentially that of a football (a soccer ball in the U.S.A.). The second common fullerene is C_{70}, which is an elongated molecule containing 12 pentagons and 25 hexagons. Figure 1 shows the structures of the C_{60} and C_{70} molecules. Generally, fullerenes are defined as closed convex cage molecules, containing only hexagonal and pentagonal faces (Dresselhaus et al., 1996; Smalley and Yakobson, 1998).

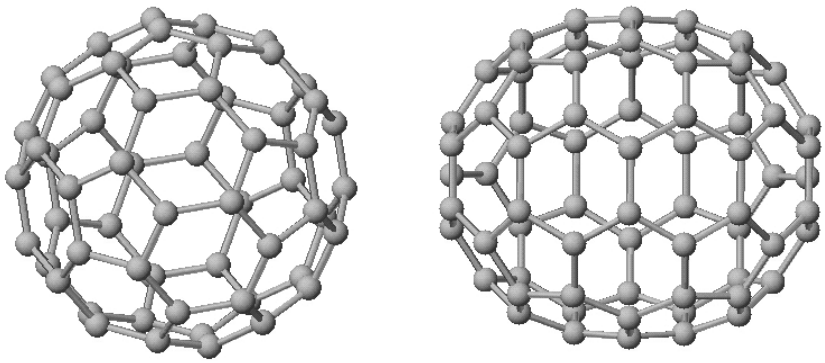

Figure 1. Structures of the C_{60} (on left) and C_{70} (on right) molecules.

Fullerenes were discovered by Kroto et al. (1985) in 1985. They produced carbon clusters by laser vaporization of carbon species from graphite into a high-density helium flow. The time-of-flight mass spectra of the carbon clusters showed a significant enhancement of carbon clusters with 60 carbon atoms, as well as of clusters with 70 atoms, but less prominently. It was suggested that the remarkably stable C_{60} cluster has a truncated icosahedral structure like a soccer ball. The structure of fullerenes has since been confirmed by nuclear magnetic resonance and other methods (Dresselhaus et al., 1996). In 1996, Robert F. Curl, Sir Harold W. Kroto, and Richard E. Smalley were winners of the Nobel Prize in Chemistry for their discovery of fullerenes.

Five years after their discovery, Krätschmer et al. (1990) developed a method to synthesize fullerenes in macroscopic amounts. They produced carbon soot with a few percent of C_{60} molecules by evaporating graphite electrodes in a helium atmosphere. Subsequently, the soot was dispersed in benzene and the fullerenes were dissolved, producing a wine-red to brown liquid. The liquid was then separated from the soot and dried, forming solid fullerene crystals. From these crystals the structure of solid crystalline fullerenes was then determined by X-ray and electron diffraction. Since then a variety of other techniques have been used to produce fullerene molecules from carbon-rich vapors, including ac or dc plasma discharge between carbon electrodes, laser ablation of carbon electrodes, and oxidative combustion of a benzene/argon gas mixture (Howard et al., 1992; Dresselhaus et al., 1996).

The discovery of the methods for producing macroscopic quantities of fullerenes stimulated a wide variety of studies of the chemistry and physics of fullerene materials. It was soon found that fullerenes and related materials have many interesting properties. One of the most significant properties is superconductivity, which was first demonstrated for potassium-doped C_{60} at 18 K by Hebard et al. (1991b). Soon superconductivity was also observed for C_{60} doped with other alkali metals or Ca (Buntar and Weber, 1996; Dresselhaus et al., 1996). Other interesting properties include non-linear optical properties, ferromagnetism, catalytic activity and ability to convert to diamond when rapidly compressed. Possible applications include catalysts, optical limiters, carbon composites, molecular sieves, and superconducting and nanoscale devices (Fleming et al., 1992; Dresselhaus et al., 1993; Rao et al., 1995; Buntar and Weber, 1996; Dresselhaus et al., 1996; Huffman, 1996). The interest in

fullerenes is also due to their peculiar geometrical shapes; the C_{60} fullerene is perhaps the most symmetric molecule. In addition, it is a very interesting compound for testing and developing crystal growth theories because the crystal structure can be regarded as a close spacing of spheres bounded by relatively weak, isotropic van der Waals forces (Verheijen et al., 1992b; Verheijen et al., 1993).

2.1.2 Solid fullerenes

Fullerenes are the third crystalline from of pure carbon, in addition to graphite and diamond. The solid form of the fullerenes is often called fullerite. In the crystal, fullerene molecules are bound together essentially by weak, isotropic van der Waals forces. The van der Waals forces between fullerene molecules are much weaker than between carbon atoms in the fullerene molecule. Therefore, the fullerene crystals are relatively soft, although the molecule itself is quite stable. Furthermore, fullerene crystals contain interstitial voids between relatively large molecules (diameter about 1 nm). It is possible that rather large molecules and atoms can be incorporated into these voids (Dresselhaus et al., 1993; Fischer, 1993; Dresselhaus et al., 1996; Huffman, 1996).

The first experiments indicated that the crystals grown from solvent have hcp (hexagonal close-packed) structure (Krätschmer et al., 1990). However, subsequent works showed that the crystal structure of pure C_{60} at ambient temperature is fcc (face-centered cubic) with a lattice constant of 14.17 Å when the crystals are formed from vapor and they do not contain any impurities. Both hcp and fcc structures are closed-packed structures. They are energetically very similar, but have a different stacking arrangements. The hcp structure has an ABABAB... stacking sequence, while for fcc it is ABCABC... (Kingery et al., 1976). In the crystal at room temperature, the C_{60} molecules are rotating randomly and rapidly. Upon cooling to about 255 K, a phase transition from fcc to a simple cubic (sc) structure occurs. The molecules cannot rotate freely anymore and they completely lose two of their three degrees of rotational freedom (Dresselhaus et al., 1993; Fischer, 1993; Dresselhaus et al., 1996; Huffman, 1996).

The crystal structure of C_{70} is more complex than that of C_{60}. It has several different crystal structures as a function of temperature. At high temperatures

(T > 340 K), the fcc structure with a lattice parameter of 15.01 Å is most stable, but the hcp structure is almost equally stable. At ambient temperature, both fcc and hcp crystals are observed to form in the vapor phase (Verheijen et al., 1992a; Dresselhaus et al., 1993; Van Tendeloo et al., 1993; Dresselhaus et al., 1996).

Defects such as stacking faults and twins frequently occur in large single fullerene crystals even if they have grown very slowly from the gas phase. The microstructure of these fullerene crystals is very similar to those of fcc metals and alloys with a low stacking fault energy (Muto et al., 1992; Van Tendeloo et al., 1992) In a stacking fault there are misplaced planes of molecules in the stacking arrangement (see Figure 10), while there is a mirror plane in the stacking arrangement in a twin boundary (see Figure 13). A stacking sequence for a stacking fault and a twin is, for example, ...ABCABABC... and ...ABCABCBACBA..., respectively (Ashcroft and Mermin, 1976).

Since the tight fullerene molecules are weakly bounded together by van der Waals forces, the mechanical properties of the solid fullerenes can be described as light, weak and soft. Solid fullerenes easily compress under the action of pressure. As for the electrical properties, the solid, pure C_{60} is a semiconductor with a large band gap of about 1.5 eV. Its electrical conductivity is very low. However, the conductivity of solid fullerenes can be increased by doping, even to such an extent that they are superconductive. As for thermodynamic properties, solid fullerenes sublimate at comparatively low temperatures (about 450 °C), and they do not have a liquid phase. (Hagen et al., 1993; Buntar and Weber, 1996; Dresselhaus et al., 1996; Huffman, 1996; Yao et al., 1997). Since fullerenes sublimate at low temperatures and are soluble in a number of organic solvents, fullerene materials in different forms can be produced easily.

2.1.3 Synthesis of fullerene crystals, particles and clusters

Solid fullerene materials have been produced in different forms: large single crystals, particles or crystals in the micrometer and nanometer size range, very small clusters and aggregates, as well as thin films.

The first crystals of solid fullerenes were grown from benzene solutions by Krätschmer et al. (1990). The fullerene crystals were micrometer-sized (up to

500 μm) and mainly rods, platelets and star-like flakes in shape. The main disadvantage in the growth of fullerene crystals and particles in the liquid phase is that solvent molecules and impurities can be incorporated into the lattice, and various crystal structures and solvate crystals can be obtained (Fleming et al., 1991a; Fleming et al., 1992; Dresselhaus et al., 1996; Ceolin et al., 1997). However, solvent-free fullerene crystals with fcc structure grown from organic solvents have also been reported (Yosida et al., 1992; Talyzin et al., 1996). The large single fullerene crystals (up to a millimeter in size) have been grown mainly from the vapor phase by sublimation, and by vapor transport methods in a vacuum or in an inert gas atmosphere in a closed or in an open tube. In addition to defect-free single crystals, twinned and multiply-twinned crystals were observed frequently (Fleming et al., 1991b; Meng et al., 1991; Verheijen et al., 1992a; Verheijen et al., 1992b; Haluska et al., 1993; Liu et al., 1993; Dresselhaus et al., 1996).

Several methods to produce fullerene particles and crystals in the nanometer size range have been reported. Ohno and Yatsuya (1998) reported the preparation of fullerene nanoparticles via the gas-evaporation technique by heating fullerene (C_{60} and C_{70}) samples to 1000–1750 °C in an argon atmosphere at 0.7–2.6 kPa pressures. Almost all of the particles had irregular external shapes with sizes from 100 to 400 nm. Only a few particles with defined crystal habits, e.g. lamellar and multiply-twinned particles, were observed. Wragg et al. (1990) prepared "smoke" particles, with sizes below 100 nm, by heating fullerene powders in a helium atmosphere at 13 kPa pressure. The particles were postulated to consist of roughly spherical microcrystals with diameters of about 20 nm. Ito et al. (1998) used a similar inert gas condensation method to produce fullerene crystals of about 50 nm in size.

Fujitsuka (1997) generated granular particles with an average diameter of 270 nm by reprecipitation of a solution of fullerenes in CS_2 and ethanol. Scrivens and Tour (1994) prepared an aqueous solution of fullerene particles by mixing a solution of fullerenes in benzene, THF and acetone with water. The particles formed by precipitation were roughly spherical and uniform in size, with an average diameter of 300 nm. In addition, Andrievsky et al. (1995) synthesized an aqueous colloidal solution of fullerenes with particle sizes from several nanometers to 220 nm by evaporating a solution of fullerenes in toluene and water.

Thin films of fullerenes have been prepared by vacuum sublimation and other methods. Epitaxial, polycrystalline and amorphous films have been grown on a variety of substrates (Hebard et al., 1991a; Krakow et al., 1993; Dresselhaus et al., 1996; Gao and Zhang, 1996; Richter et al., 1997). Fullerene particles and crystals may be grown during the initial stage of the thin film growth processes. The formation of fullerene nanoparticles and nanocrystals during the thin film growth on various substrates, e.g, on NaCl, KI, mica and GaAs, has been reported in numerous papers (Li et al., 1991; Saito et al., 1993; Tanigaki et al., 1993; Lüthi et al., 1994a; Yanagi and Sasaki, 1994). The diameters of the particles varied from a few nanometers up to micrometers, and different morphologies were observed: e.g. irregular shapes, hexagonal and triangular plates as well as multiply-twinned particles (Saito et al., 1992; Zhou et al., 1993).

Fullerene clusters and aggregates consisting of several molecules were reported to have been formed in the gas phase (Martin et al., 1993) and in organic solutions (Ying et al., 1994; Ahn et al., 1998) as well as at early stages of nucleation during a thin film growth (Janda et al., 1998). Jensen and Sorensen (1996) discussed the formation of fullerene clusters by depositing coatings via electrospraying.

2.1.4 Applications of fullerene nanomaterials

Fullerene nanomaterials have many possible applications. For instance, fullerene and fullerene-based nanomaterials can be used as carrier materials for drugs, isotopes and antibodies in medicine (Scrivens and Tour, 1994; Kolari et al., 1996), as high surface area particles and supports in catalysis (Ichinose et al., 1992; Dresselhaus et al., 1996), as an electron beam resist for lithography (Tada and Kanayama, 1996), as sensor materials (Saab et al., 1998), and in optical and electronic devices (Haddon et al., 1995; Tanigaki, 1995). Fullerenes can also be used as source material for carbon-based (e.g. amorphous and diamond-like) coatings and other nanostructures (Dresselhaus et al., 1996; Huffman, 1996; Milani and Manfredini, 1996).

Ultrafine fullerene nanoparticles can be used in medical applications for studies and treatment involving the lymphatic system. The best absorption from interstitial space to the lymphatic system seems to be achieved with particle

sizes of 30–50 nm. An optimal nanoparticle could be also used for visualization *in vivo*, as a carrier material for drugs, isotopes and antibodies, and for contrast enhancement (Kolari et al., 1995; Kolari et al., 1996).

Since fullerene nanocrystals can be moved on a substrate with a scanning force microscope, Lüthi et al. (1994b) proposed that fullerene nanocrystals could be used in the field of nanotechnology. For instance, fullerene nanoparticles with a well-defined shape could be used as transport devices for fabrication processes of nanometer-size machines.

2.2 Materials processing

Aerosol synthesis methods have been applied for the production of nanostructured fullerene particles in this thesis. In this chapter, nanostructured materials and aerosol processing routes for material production are briefly described. In addition, a short summary of the aerosol synthesis of fullerene particles is given.

2.2.1 Nanostructured materials

Nanostructured materials are generally defined as materials having a characteristic length scale of typically less than about 100 nm in at least one dimension. The length scale can be a particle diameter, a grain size or a layer thickness. These materials are also known as nanocrystalline and nanophase materials, and the particles as ultrafine particles and nanoparticles. Nanostructured materials have interesting and possibly useful mechanical, physical, optical, electrical and magnetic properties (see reviews Gleiter, 1989; Gleiter, 1992; Siegel, 1993; Suryanarayana, 1995; Edelstein and Cammarata, 1996).

Nanostructured materials with a grain or particle size of 1–20 nm have a large volume fraction of atoms at their grain boundaries or particle surfaces. As a result of such microstructure, several properties of nanostructured materials differ from those of bulk or coarse-grained materials. The sintering and densification temperatures of nanophase ceramics and metals are lower than those of conventional materials, and they can deform easily at low temperatures.

They can be fabricated to be stronger, tougher and harder than their conventional forms. Nanostructured ceramics can be elastic or even superplastic. Nanocrystalline or nanometer-size particles with very high surface areas can have significant reaction rates and improved catalytic selectivity in catalytic applications. In addition, metallic nanoparticles can be used as components in single-electron devices in electronics (Gleiter, 1989; Ichinose et al., 1992; Siegel, 1993; Suryanarayana, 1995; Edelstein and Cammarata, 1996).

Nanostructured materials can be produced in the gas phase, e.g. by gas condensation from supersaturated vapor, in the liquid phase, e.g. by chemical methods, and in solid state, e.g. by mechanical attrition. The synthesis techniques for nanostructured materials include inert-gas condensation, sputtering, plasma processing, vapor deposition, sol-gel, electro-depositing, rapid quenching, crystallization of amorphous solids, and mechanical milling/ alloying (Gleiter, 1989; Uyeda, 1991; Ichinose et al., 1992; Siegel, 1993; Li et al., 1994; Suryanarayana, 1995; Edelstein and Cammarata, 1996). Aerosol synthesis methods can also be used to produce materials that contain, or that are composed of, particles or grains in the nanometer size range. Therefore, aerosol routes are promising for the production of nanostructured materials (Kodas and Hampden-Smith, 1999).

2.2.2 Aerosol processing of materials

Aerosol processing methods are commonly used to generate a wide variety of materials such as metals, metal oxides, non-oxide ceramics, semiconductor and superconducting materials as well as nanostructured materials. Aerosol methods can be used to produce high-purity powders with controlled crystallinity and particle size (Kodas, 1989; Gurav et al., 1993b; Messing et al., 1993; Pratsinis and Kodas, 1993; Kruis et al., 1998; Pratsinis, 1998; Kodas and Hampden-Smith, 1999).

Aerosol routes in material processing can be classified into gas-to-particle and droplet-to-particle conversions. In the gas-to-particle conversion route, particles are formed from supersaturated vapor of a condensable species in a carrier gas. Supersaturated vapor is formed either as a result of chemical reactions which create new molecules, or physical processes, such as cooling which reduces the saturation vapor pressure of the condensable species. At a sufficiently high

supersaturation, new particles are formed by nucleation, which is followed by particle growth via condensation, coagulation and agglomeration. Generally, particles produced by gas-to-particle conversion have a relatively narrow size distribution and consist of solid, spherical primary particles. However, hard agglomerates are often formed and it can be difficult to produce multicomponent particles with homogeneous chemical composition. The gas-to-particle conversion route has been used for the production of metals (e.g. Ag, Au, Cu, Mo), oxide and non-oxide ceramics (e.g. Al_2O_3, TiO_2, SiO_2, MgO, AlN, BC), and semiconductors (e.g. GaAs, ZnS). Furthermore, nanostructured materials and nanoparticles are relatively easy to produce by the gas-to-particle route, since the primary particle size is generally small, from several nanometers to micrometers, depending on the process. On an industrial scale, titania, fumed silica and carbon blacks are produced using this method (Scheibel and Porstendörfer, 1983; Kodas, 1989; Gurav et al., 1993b; Pratsinis and Kodas, 1993; Kodas and Hampden-Smith, 1999).

In the droplet-to-particle conversion route, precursor solution droplets are suspended in gas by liquid atomization. These droplets are converted to powder by drying, by direct pyrolysis or by in situ reactions with carrier-gas components. Aerosol decomposition (i.e. spray pyrolysis) and aerosol droplet/ spray drying are the most common processes for the generation of powders from liquid-phase precursors. These processes involve the atomization of the precursor solution into droplets, which are then carried through a furnace by a carrier gas. Inside the furnace the solvent evaporates from droplets, and precursor precipitation occurs to form dry precursor particles. In the case of spray pyrolysis, this is followed by intraparticle reaction of the precursors within the dried particles to form the product powder and gaseous reaction products. Generally, organic and inorganic materials as well as multicomponent particles with high purity and uniform chemical composition can be produced via droplet-to-particle route. In addition, unagglomerated spherical particles with controlled size can be generated. However, porous, hollow particles are often formed and the spread of the particle sizes is limited by the spread of the generated droplets. Furthermore, phase segregation may occur for multicomponent particles. The droplet-to-particle conversion routes have been used for the production of metals (e.g. Ag, Au, Cu, Ni, Pd), simple metal oxides (e.g. CuO, Fe_2O_3, Fe_3O_4, SnO_2, V_2O_3), complex metal oxides (e.g. mullite, $NiFe_2O_4$, $BaTiO_3$), superconductors (e.g. $YBa_2Cu_3O_{7-x}$, Bi-Sr-Ca-Cu-O) and

non-oxide ceramics (e.g. AlN, BN, ZnS). On an industrial scale, simple and complex metal oxides are produced (Kodas, 1989; Gurav et al., 1993b; Messing et al., 1993; Pratsinis and Kodas, 1993; Kodas and Hampden-Smith, 1999).

The droplet-to-particle conversion route can be also used for the production of nanostructured materials. A particle may consist of many nanometer-sized crystallites although the particle diameter can be much larger. During the production the grain size of the particles can be kept small by operating at temperatures which are sufficient for complete drying (aerosol droplet drying) and decomposition (aerosol decomposition) of precursors, but not high enough to cause excessive grain growth. For instance, the aerosol decomposition route has been used for the production of nanostructured PdO, V_2O_5, Fe_3O_4 and $YBa_2Cu_3O_{7-x}$ particles and $YBa_2Cu_3O_{7-x}$/Ag nanocomposites (Kodas, 1989; Lyons et al., 1992; Gurav et al., 1993b; Pratsinis and Kodas, 1993; Joutsensaari and Kauppinen, 1997).

2.2.3 Aerosol synthesis of fullerene particles

Fullerene particles studied in this thesis have been produced by aerosol synthesis methods. Since fullerenes are soluble in a range of organic solvents (e.g. toluene and benzene) (Sivaraman et al., 1992; Ruoff et al., 1993) and have appreciable vapor pressures above 500 °C (Baba et al., 1994; Piacente et al., 1995; Piacente et al., 1996), both droplet and vapor phase aerosol routes can be applied to produce fullerene or fullerene-based particles. Gurav et al. (1993a) introduced the production of nanostructured fullerenes and fullerene-rhodium nanocomposites. Nanostructured fullerene particles were generated by aerosol droplet drying of a mixed fullerene solution in toluene using N_2 as a carrier gas at a processing temperature of 200 °C. The particles were polycrystalline with a small crystallite size of roughly 10 nm. Fullerene-Rh nanocomposites were produced by aerosol decomposition (i.e. spray pyrolysis) of fullerene solution and Rh precursor in toluene at 550 °C. The particles formed were nanocomposites with a crystallite size of about 4 nm and 10 nm for rhodium and C_{60} respectively.

In a following study the generation of the fullerene nanoparticles via vapor condensation in a continuous flow system was introduced (Paper I; Gurav et al., 1994). Recently, formation mechanisms and crystallite growth of fullerene

particles during the aerosol synthesis of nanostructured fullerene particles have been further studied, starting from the atomized fullerene-toluene solutions. (Papers II–VI). The studies on formation and crystallization of fullerene particles and their mechanisms during the aerosol synthesis are described in Papers I–VI and the results are summarized and discussed in this overview.

3. Methods

Fullerene particles studied in this thesis were produced both by gas-to-particle and droplet-to-particle conversion routes, i.e. from fullerene vapor via vapor condensation and from fullerene-toluene droplets via aerosol droplet drying. In this chapter, particle production experiments and characterization methods as well as fluid dynamics and fullerene particle evaporation calculations are described briefly. They are discussed in the papers in detail.

3.1 Fullerene particle production

Four different types of experiments were carried out to produce fullerene particles and to study their formation and crystallization mechanisms. In the first experiments ultrafine fullerene particles were produced via vapor condensation, starting from fullerene powders that were vaporized in tubular flow reactors (Paper I). The experimental set-up is shown in Figure 1 in Paper I. Batches of pure C_{60} (purity 99.5 %) or mixed fullerene extract (MFE, 85 % C_{60} and 15 % C_{70}) were loaded at the center of the hot zone of the reactor and then heated to 400–600 °C to generate fullerene vapor. The fullerene vapor was carried though the reactor using nitrogen as a carrier gas. When the fullerene vapor was cooled at the reactor exit, ultrafine fullerene particles were formed.

In the rest of the experiments (Papers II–VI), fullerene particles were generated via aerosol droplet drying, starting from droplets of fullerenes in toluene. The experimental set-up is shown in Figure 2. The precursor solutions were atomized to droplets of about 700 nm in diameter by a constant output atomizer using nitrogen as a carrier gas. Subsequently, the toluene was vaporized from initial aerosol droplets, forming dry particles in the reactor inlet followed by crystallization of the particles at the heated zone and the reactor outlet. In the second set of experiments (Paper II), mixed fullerene extract (MFE, 84 % C_{60} , 15 % C_{70} and 1 % higher fullerenes) was used as the starting material. Pure C_{60} (purity >99.5 %), pure C_{70} (>98 %) and mixed fullerene (MF, 50 % C_{60} and 50 % C_{70}) particles were generated in the third set of experiments (Papers III–V), and pure C_{60} (purity >99.5 %) in the fourth set of experiments (Paper VI).

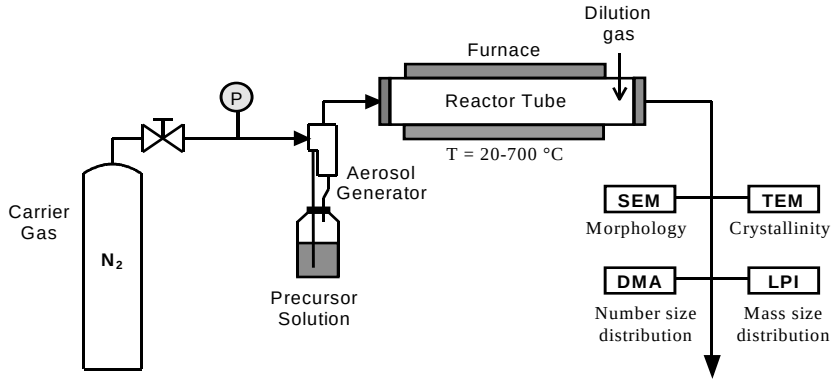

Figure 2. Experimental setup for production of nanostructured fullerene via aerosol droplet drying (Paper III).

In all experiments, particles were generated in tubular reactors with laminar flow, using nitrogen as a carrier gas at ambient pressure. Basically, two different types of laminar flow reactors were used in the studies: a large-scale (Papers I–V) and a small-scale reactor (Paper VI). The large-scale reactor design was adapted from the one used by Gurav et al. (1993a). The reactor consisted of a mullite tube with an inner diameter of 8 cm and a heated length of 91 cm in a three-zone furnace. A carrier-gas flow rate of 3 l/min was normally used (Papers II–V). In the experiments where particles were generated via vapor condensation (Paper I), flow rates of 1.5–10 l/min were used. The latest experiments (Paper VI) were carried out in the small-scale reactor with a mullite tube of inner diameter of 2.2 cm and a heated length of 60 cm, using a low aerosol flow rate of 0.3 l/min (see Figure 1 in Paper VI). The previous experiments (Papers III–V) indicated that particles with different morphologies can be formed due to non-uniform temperature and flow profiles. Thus, the small reactor was designed and constructed to achieve uniform conditions for particle synthesis. The direction of the flow was horizontal in the both reactors.

In addition, some experiments were carried out using monodisperse (size-classified) aerosols (Paper VI). The monodisperse aerosols were classified with a differential mobility analyzer (DMA) from the polydisperse aerosols.

3.2 Fullerene particle characterization

The number-size distributions of the particles (Papers I–VI) were determined in the gas phase by a differential electrical mobility analyzer (DMA) (Knutson and Whitby, 1975; Wang and Flagan, 1990; Reischl, 1991), and the mass-size distributions of mixed fullerene particles (Paper III) by a multi-stage low-pressure impactor (LPI) (Berner and Lürzer, 1980; Berner, 1984; Kauppinen and Pakkanen, 1990; Hillamo and Kauppinen, 1991). The principles of the DMA and the LPI are described briefly in Paper III. In the DMA the particles are classified according to their mobility diameter which, for non-porous particles, is essentially the Stokes diameter. For a spherical particle, the Stokes diameter is equivalent to the actual physical diameter. The impactor classifies the particles based on their aerodynamic diameter. By comparing the volume-size distributions calculated from the DMA results to the LPI mass-size distributions plotted as a function of the Stokes diameter, particle density can be estimated as in the studies in Paper III.

The C_{60}/C_{70} ratio as a function of particle size was determined from the size-classified impactor samples for the mixed fullerene particles (Paper III). The HPLC (high performance liquid chromatography) method (Van Cleempoel et al., 1996) was utilized to detect C_{70} and to determine the C_{60}/C_{70} ratio of the particles collected at the different impactor stages.

The particle morphology was studied by scanning electron microscopy (SEM). The recent SEM analyses were carried out with a low acceleration voltage (0.9–3 kV) without any conductive sample coating, in order to visualize the structures on the particle surfaces (Papers III–VI). The surface structure of the particles gives an indication of particle crystallinity. The crystal structure and crystallinity of fullerene particles were studied in detail by transmission electron microscopy (TEM), by high resolution electron microscopy (HREM) and by electron diffraction (ED) (Kirkland et al., 1990; Marks, 1994; Williams and Carter, 1996; Amelinckx et al., 1997). Most of the samples for electron microscopy were obtained by collecting particles directly on a holey (or lacy) carbon-coated copper grid by an electrostatic precipitator sampler.

3.3 Modeling of reactor conditions and fullerene particle evaporation

To further clarify the transformation and crystallite growth mechanisms of fullerene particles, the reactor conditions and evaporation of fullerene particles during the particle synthesis were modeled. The calculations were carried out for the small-scale reactor and they are described in detail in Paper VI.

Computational fluid dynamics (CFD) calculations were used to examine the effects of flow development, heat transfer and buoyancy on particle trajectories for the reactor used in the experiments (Paper VI). The reactor flow and temperature fields were calculated using the commercial Fluent CFD package. Furthermore, evaporation rates of the fullerene particles during the synthesis were calculated in order to estimate the concentration of fullerene vapor in the gas phase at the heated zone of the reactor (Paper VI). The evaporation of the particles was calculated using a diffusional transport equation (eq. 1 in Paper VI) according to Flagan and Seinfeld (1988).

4. Results and discussion

The main results of Papers I–VI are summarized in this chapter. The experiments show that it is possible to produce particles with controlled crystallinity and morphology. The formation and crystallization mechanisms of fullerene particles during aerosol synthesis are discussed in detail in this chapter.

4.1 Particle production conditions

In this chapter, conditions for fullerene particle production during particle synthesis are discussed. The results from the CFD calculations and the improvements in the reactor set-up design are discussed. Finally, the particle production conditions of the aerosol methods used in this study are compared to other methods for producing fullerene particles.

4.1.1 Reactor design and fluid dynamics

In order to achieve more uniform conditions for particle production, the small-scale reactor set-up was designed and used in the recent study (Paper VI). The set-up has been improved in several ways when compared with the large-scale ones that were used previously (Paper I–V). A smaller reactor tube, a slower cooling rate after the heated zone, and a connections with low angle expansion/ restriction between the reactor tube and the piping have been introduced. This can significantly affect both particle formation and crystallite growth mechanisms.

The flow and temperature fields of the small-scale reactor were examined by CFD calculations. The results of the CFD calculations (Paper VI) show (see Figure 2 in Paper VI) that the flow has large recirculation regions at the inlet and outlet of the heated zone when the gas is rapidly heating or cooling. However, the flow and temperature profiles as well as the residence time histories of the particles at the maximum temperature are uniform within the heated zone. The minimum residence time in the center of the reactor tube is at least several seconds for all particles. It is noteworthy that many processes, e.g. grain growth and particle vaporization, are exponentially related to the

temperature and linearly to the residence time. To summarize, the CFD calculations show that uniform conditions, especially regarding the temperature and flow profiles and the residence times in the heated zone, can be achieved in a small tubular aerosol reactor using a low aerosol flow rate. This indicates that particles with relatively homogeneous crystallinity and morphology can be produced.

4.1.2 Comparison with other methods

In comparison with other particle production methods, e.g. precipitation in liquids, or gas-evaporation techniques, aerosol flow reactor techniques have several advantages (Paper V). With careful reactor design, the temperature and flow profiles are uniform and the residence times for particle formation and crystallization are longer. Thus particles with more uniform crystallinity, morphology and size can be produced. Moreover, particles with high purity and uniform crystallinity can be produced, whereas in liquid phase processes solvent molecules can affect the crystallinity of the particles (Dresselhaus et al., 1996). When particles are formed during thin film growth, the substrate may contribute to particle formation and crystal growth. In aerosol flow reactors, the particles are formed in an inert atmosphere, and the formation and crystal growth mechanisms are easier to clarify and understand. Finally, the aerosol flow reactor methods are continuous processes, whereas many other production methods are batch processes.

4.2 Fullerene particle formation and densification

Fullerene particles were produced by the vapor condensation method starting from fullerene vapor, and by the aerosol droplet drying method starting from fullerene-toluene droplets. The condensation method resulted in ultrafine particles with diameters of 30–60 nm, whereas the droplet-to-particle method was mainly used to produce larger particles with a diameter of around 100 nm. In this chapter the formation mechanisms and the densification of fullerene particles during the aerosol synthesis are discussed based on particle size distribution measurements and particle vaporization calculations In addition, the possibility of separating different fullerenes when particles are produced from droplets of C_{60} and C_{70} in toluene are discussed.

4.2.1 Particle formation mechanisms and densification

Fullerene particles can be produced by both gas-to-particle and droplet-to-particle aerosol routes. In the vapor condensation method, ultrafine fullerene particles were produced by vaporizing fullerene powders in a continuous flow reactor (Paper I). The mechanisms occurring during particle formation are shown schematically in Figure 2 in Paper I. Since fullerenes are volatile at 400 °C and have appreciable vapor pressures above 500 °C (Baba et al., 1994; Piacente et al., 1995), fullerene evaporates when the reactor is heated to 500 °C and above. The fullerene vapor cools while exiting the heated zone of the reactor, thereby increasing the saturation ratio, which lead to the formation of new particles via homogeneous nucleation. The critical radius is estimated to be several nanometers, depending on the cooling rate (Seker et al., 1996). Subsequently, the particles are grown by condensation and agglomeration.

Figure 3 shows the number size distributions for C_{60} particles produced at different reactor temperatures via vapor condensation. The results show that ultrafine (30–60 nm) fullerene particles can be produced by vapor condensation. The sizes of the fullerene particles can be controlled by varying the reactor

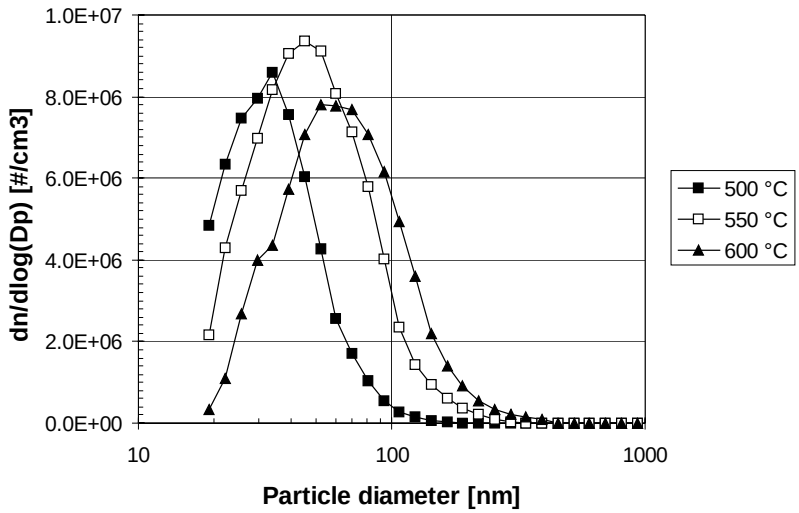

Figure 3. Number size distributions for C_{60} particles produced at different reactor temperatures via vapor condensation.

temperature and the cooling rate at the reactor exit. For instance, the geometric mean diameter increases monotonically from 30 nm to 60 nm when the reactor temperature is raised from 500 °C to 600 °C. Such an increase in the particle size as well as in the total particle concentration with increasing temperature is caused by the increasing amount of fullerene vapor generated at higher tempesratures due to the increased vapor pressure (Paper I).

In the aerosol droplet drying method (Papers II–VI), the fullerene particles with diameters of about 100 nm are formed from fullerene-toluene droplets by drying and crystallization. The mechanisms occurring during particle formation are shown schematically in Figure 6 in Paper III. In this case, the toluene (solvent) is vaporized from the initial aerosol droplets, forming dry particles in the reactor inlet. This is followed by densification and crystallization of the particles in the hot zone of the reactor. The particle-size distribution measurements show that the average particle size reduces when the reactor temperature rises from room temperature to 400 °C, as shown in Figure 4. The reduction in the particle size is mainly due to particle densification and crystallization. DMA-impactor

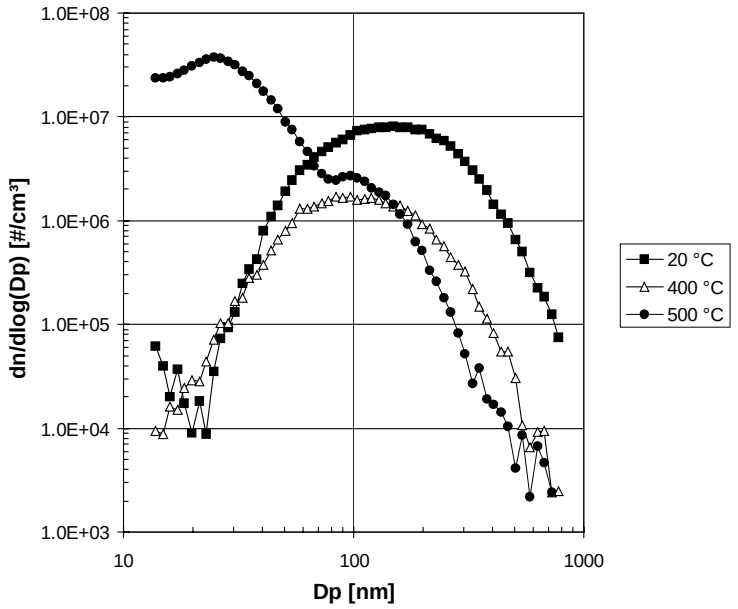

Figure 4. Number size distributions of mixed fullerene particles for processing temperatures of 20 °C, 400 °C and 500 °C (Paper II).

comparison results (Paper III) indicate that the density of mixed fullerene particles (50 % C_{60} and 50 % C_{70}) monotonically increased from 1.1 to 1.6 g/cm^3 when raising the reactor temperature from 400 °C to 700 °C. At higher temperatures (600–700 °C), the particle density is close to the bulk density of C_{60} and C_{70} (1.7 g/cm^3) (Dresselhaus et al., 1996), indicating that almost completely dense fullerene particles can be produced (Paper III).

At higher temperatures (500–600 °C), the results show that two types of particles in the different size ranges are formed: larger particles with diameters of about 100 nm and ultrafine particles with diameters of about 30 nm (Figure 4). This indicates that the fullerene particles are partially vaporized and new ultrafine particles are formed via homogeneous nucleation, and subsequently grown by condensation when fullerene vapor is cooled at the reactor exit. However, the particle size distribution is unimodal and quite narrow (see Figure 6d in Paper VI) for particles with a high initial mass concentration (78 mg/m^3) produced under the controlled conditions at 500 °C (Paper VI). This indicate that fullerene is mainly vaporized from the particles and subsequently condensed back onto surfaces of the residual particle as in evaporation-condensation monodisperse aerosol generator (Hinds, 1999).

The evaporation calculation results (Paper VI) for polydisperse particles having a higher mass concentration (15–78 mg/m^3) show that the amount of fullerene vapor in the gas phase in the heated zone increased from a few percent to 100 % when the gas temperature increased from 400 °C to 500 °C (see Figure 5). This indicates that a major fraction of fullerene is vaporized during the synthesis. It should be noted that the calculations were stopped at the end of the heated zone, i.e. the current model simulates only fullerene particle evaporation in the heated zone of the reactor. Furthermore, in the calculations the fullerene particles were assumed to be monodisperse perfect spheres with smooth surfaces whereas the actual particles were solid with mainly irregular shapes and rough surfaces. Some of the particles were even perfectly faceted.

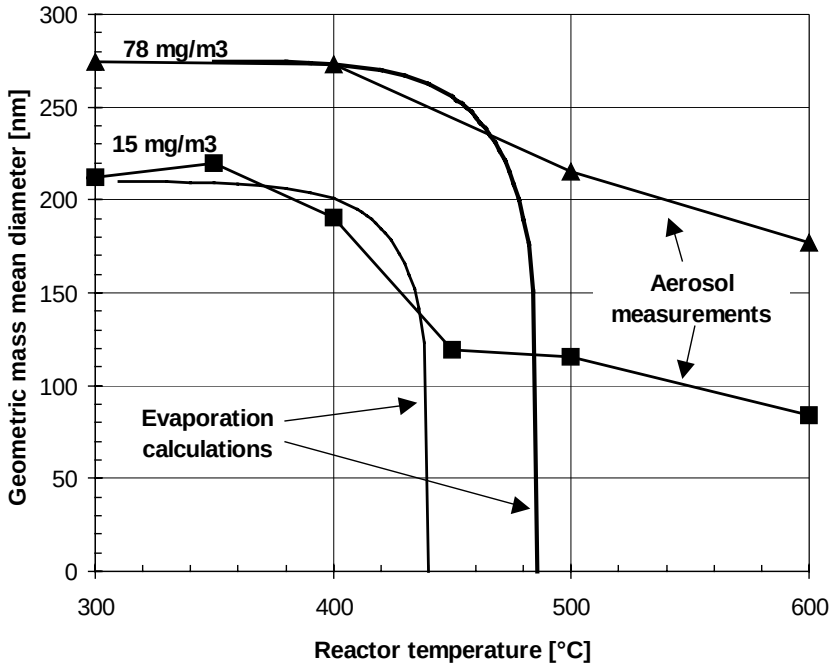

Figure 5. Evolution of geometric mass mean diameter of polydisperse particles with low (15 mg/m^3) and high (78 mg/m^3) particle mass concentration at different temperatures according to evaporation calculations and experimental results. Evaporation of the particles was only calculated in the heated zone of the reactor. Particles were assumed monodisperse in the calculations (Paper VI).

4.2.2 Separation of mixed fullerenes

The C_{60}/C_{70} ratio of the size-classified mixed fullerene (50 % C_{60} and 50 % C_{70}) particles collected at the different impactor stages, and of the filter samples were determined by the HPLC (high performance liquid chromatography), in order to understand the vaporization and subsequent new particle formation and condensation in a binary system of fullerenes (Paper III). Only a slight differences in the C_{60}/C_{70} ratio between different impactor stages were observed. In addition, overall impactor and filter results show that the average particle C_{60}/C_{70} ratio does not change with different reactor operating temperatures. This indicates that only minor fractionation occurs during the synthesis of mixed fullerene particles. This is due to the small differences in partial vapor pressures

(Baba et al., 1994). Furthermore, C_{60} and C_{70} molecules are fully miscible in the crystals of the particles (Paper IV). The results show that it is difficult to separate different fullerenes by aerosol droplet drying, vaporization of fullerenes and subsequent vapor condensation when starting from C_{60}–C_{70} solution droplets.

4.3 Particle crystallinity, morphology and transformation

The crystallinity and crystal structure of the particles are discussed in this chapter. The results show that the fullerene particles are nanocrystalline at 20–200 °C, polycrystalline at 300–400 °C and single crystals at 500–600 °C (Papers II–VI). At processing temperatures of 500 °C and above, particles with clearly faceted shapes were observed (Papers III–VI). The most common shapes among perfectly faceted particles were hexagonal plate-like, decahedral and icosahedral (see Figure 6). The plate-like particles are lamellar-twinned and the decahedral and icosahedral particles are multiply-twinned. The structure and growth mechanisms of lamellar and multiply-twinned particles as well as the theoretical shape of fullerene particles is discussed in detail in this chapter. Finally, the transformation and growth mechanisms of faceted fullerene particles during the aerosol synthesis are discussed (Paper VI). The results base mainly on our HREM results of the fullerene particles as well as on the result for other materials and fullerenes produced via various synthesis methods.

4.3.1 Particle crystallinity and crystal structure

The crystallinity and morphology of fullerene particles mainly depend on the processing temperature. The electron microscopy results indicate that C_{60} particles are roughly spherical, having pores and voids at temperatures of 300 °C and below (Paper VI). The particles are already crystalline and likely to be fine-grained at 20 °C and they are polycrystalline at temperatures up to 300 °C. At 400 °C, the polydisperse particles are crystalline, but sometimes heavily faulted. Smaller particles with sizes of around 100 nm and below are single crystals and sometimes clearly faceted. At 500 °C and above, larger C_{60} particles are mainly single crystals when processed in controlled conditions (Paper VI), whereas the particles are highly disordered (mostly polycrystalline) or single crystals, some of them being clearly faceted, when processed in less

a)

b)

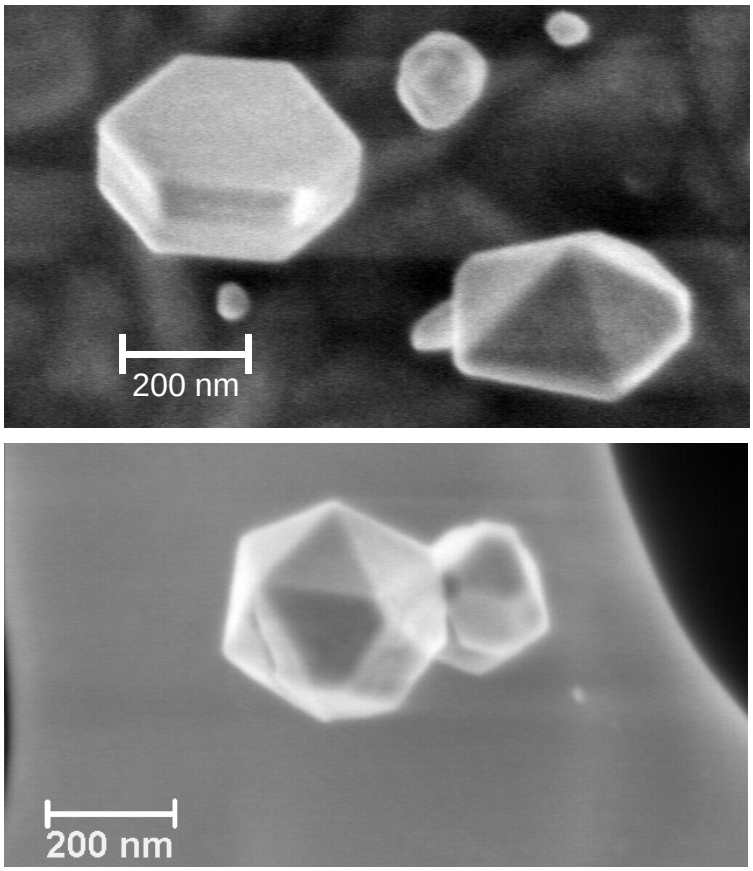

Figure 6. SEM images of a) hexagonal plate-like (particle on left), decahedral (particle on right) (Paper IV) and b) icosahedral fullerene particles.

controlled conditions (Papers III–V). At 600 °C the particles are mostly single crystals and some of them are perfectly faceted.

Similar results are observed for the C_{70} and the mixed fullerene particles. However, they are less crystalline at the same processing temperatures (Papers II–V). For instance, crystallites with a size of a few nanometers are already formed at 200 °C for particles produced from mixed fullerene extract (84 % C_{60}, 15 % C_{70} and 1 % higher fullerenes). The size is increased to about 20–30 nm at 500 °C (Paper II).

The particle crystallinity can be controlled by varying the reactor operating temperature during the aerosol synthesis. Of course the residence time in the heated zone also contributes to the particle crystallinity. The effect is, however, less significant (Gurav et al., 1996). In short, fullerene particles are nanocrystalline at 20–200 °C, polycrystalline at 300–400 °C and single crystals at 500–600 °C. The grain size can be kept small by operating at sufficiently low temperatures where grain growth is minimized. Roughly the same crystallization sequence has previously been observed for metal oxides, but at higher temperatures (Lyons et al., 1992; Joutsensaari and Kauppinen, 1997). The mechanisms occurring during particle crystallization are shown schematically in Figure 15 in Paper VI.

The ultrafine fullerene particles formed via vapor condensation are mostly polycrystalline, solid, and spherical in shape for all fullerenes at 500 °C (Papers I, IV and V). In addition to polycrystalline particles, some (defected) single crystals are observed at 600 °C. When ultrafine particles are formed at the end of the reactor during gas cooling, their residence time is too short (a few seconds) to form perfect crystals. Furthermore, the growth rate of the fullerene particles is quite fast due to high supersaturation of the fullerene vapor at the reactor outlet.

The crystal structure of the fullerene particles produced by aerosol droplet drying was determined by electron diffraction (ED) analysis (Paper IV–VI). The results show that the structure of well-crystallized C_{60}, mixed fullerene (50 % C_{60} and 50 % C_{70}) and C_{70} particles is fcc with lattice constants of 1.41 nm, 1.43 nm and 1.47 nm, respectively (Paper IV). The intermediate lattice parameter of mixed fullerene particles indicates that the particles are solid solutions of C_{60} and C_{70}, i.e. C_{60} and C_{70} molecules are fully miscible in the crystal lattice of the fcc phase. Previous studies indicated that the solid solution crystals of C_{60} and C_{70} can be formed both by condensation from the vapor phase (Kniaz et al., 1995) and by crystallization in the solution (Baba et al., 1994). Our results indicate that fullerene alloys can also be produced via aerosol synthesis methods (Paper IV).

4.3.2 Equilibrium morphology of fullerene particle

The crystal habit of the particles depends on the crystal composition, the structure of the crystal, and the growth conditions, as well as on the kinetics of growth. If the kinetics of growth dominate then the shape is determined by the growth rates on the different crystal faces. The predicted morphology depends on the relative growth rates in the different crystallographic orientations. Generally, the faces that grow fast disappear and the slow-growing ones remain. If the particles are formed in thermal equilibrium, their shape results from minimizing the surface energy (El-Shall and Edelstein, 1996; Liu and Bennema, 1996). Verheijen et al. (1992a; 1992b) have predicted theoretical equilibrium shapes for fcc (face-centered cubic) C_{60} and C_{70} crystals that are grown slowly from the vapor phase, based on the periodic bond chain (PBC) theory (Hartman and Perdok, 1955c; Hartman and Perdok, 1955a; Hartman and Perdok, 1955b). The equilibrium morphology of an fcc C_{60} and C_{70} crystal is an octahedral shape of {111} faces truncated by {100} faces at the corners as shown in Figure 7. A similar shape is also predicted for many fcc metals (Uyeda, 1991).

Particles with the truncated octahedral shape have only occasionally been observed in the present study. Figure 7 shows a SEM image of a C_{70} particle

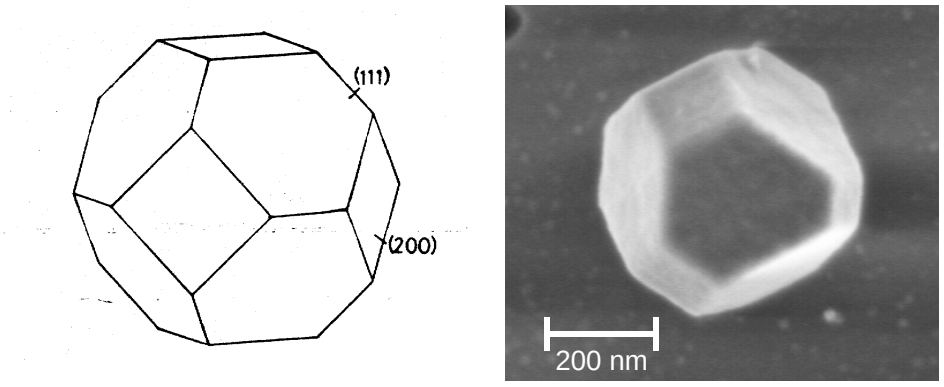

Figure 7. The equilibrium morphology of an fcc C_{60} and C_{70} crystal (left) (Verheijen et al., 1992b). It is an octahedral shape of {111} faces truncated by {100} faces at the corners. SEM image (right) of a C_{70} particle with such a crystal shape.

with just such a crystal shape. Apparently, the equilibrium crystal morphology has not yet been reached because the average residence time is only from a few seconds to tens of seconds for crystal growth in the heated zone, and even much shorter in the reactor exit, where the gas cools down and nucleation and condensation occurs. Furthermore, many of the particles with a clear faceted shape have defects such as stacking faults and twins that can promote crystal growth (Papers IV–VI). This indicates that the kinetics of growth dominates crystal formation of the faceted fullerene particles during aerosol synthesis.

4.3.3 Lamellar twinned particles

The hexagonal plate-like shape is the most common shape of clearly faceted fullerene particles (see Figure 6a). Under certain conditions (Paper VI; PD-high at 500 °C) almost all particles are hexagonal platelets. The hexagonal particles are often lamellar-twinned and have twin boundaries parallel to the extended {111} surface (Papers IV–VI). Re-entrant (groove) and convex (ridge) corners at the twin boundaries were found on the side-faces of the particles (see SEM image in Figure 6a, TEM and HREM images in Figure 8). The particles are likely to grow rapidly on the side-faces in the direction parallel to the twins, while the close-packed {111} faces grow relatively slowly. The grooves can act as favorite nucleation sites for the growth of a new molecular layer in the hexagonal particles.

Generally, the local vapor pressure is not the same at all locations over the crystal surface of faceted particles (Rogers and Yau, 1989). Over the large flat surface (111) of the platelet particles, the local vapor pressure and also the evaporation-condensation rate can be significantly different from that over the re-entrant corner on the side face of the particle (see Figure 8 above). If the curvature of the re-entrant corner is concave, the local vapor pressure over it is lower than that over a flat surface (reverse Kelvin effect), and thus the re-entrant corner is a sink for the vapor. This implies that small spherical particles disappear due to higher evaporation (the Kelvin effect), that flat surfaces remain relatively stable and that surfaces with re-entrant corners and/or other defects grow under certain conditions (Paper VI).

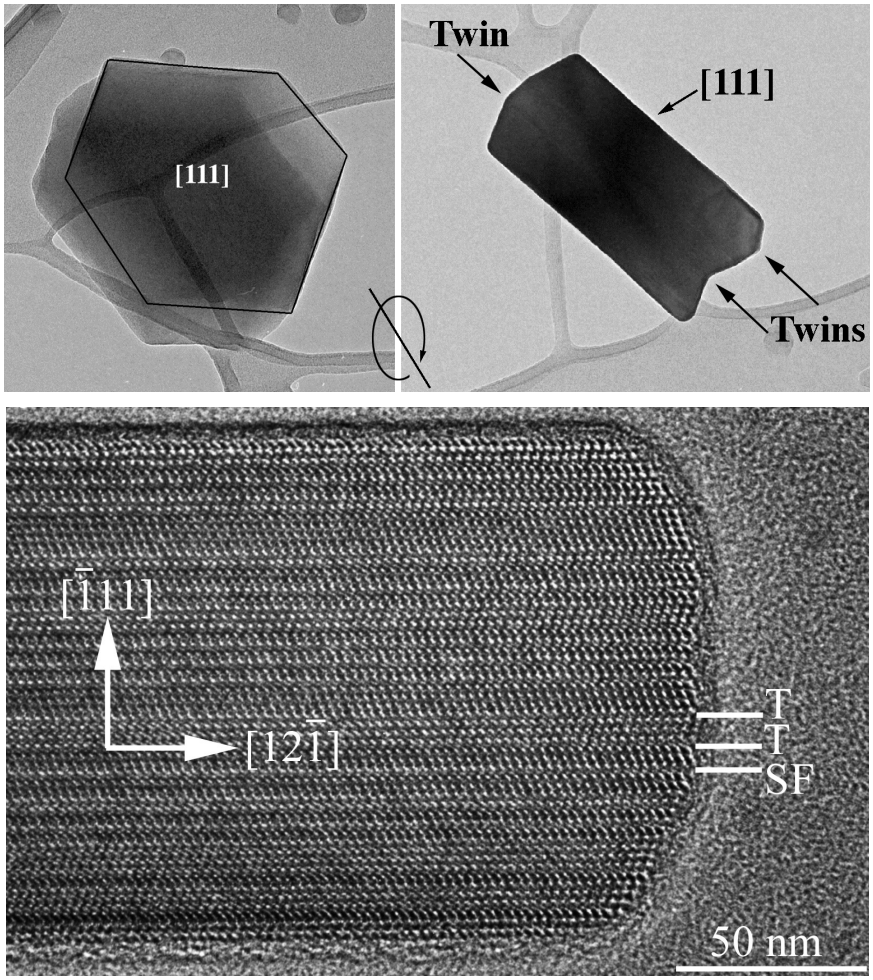

Figure 8. TEM (above) and HREM (below) images of lamellar twinned particles (Papers V and VI). HREM image shows the presence of several microtwins and stacking faults. Examples of twins are marked with T and an example of a stacking fault is marked as SF on the image below.

The crystal growth mechanism of lamellar-twinned particles on a molecular or atomic scale is more complicated (see e.g., Ming and Sunagawa, 1988; van de Waal, 1996). Figure 9 illustrates the growth of crystal by the re-entrant corner growth mechanism (van de Waal, 1996). The coordination number of a new molecule (number 1 in Figure 9b) on a perfect {111} surface is three, while it is four in a re-entrant corner (number 3 in Figure 9b) of the hexagonal plate-like particle with lamellar twins. This means that a new fullerene molecule is more

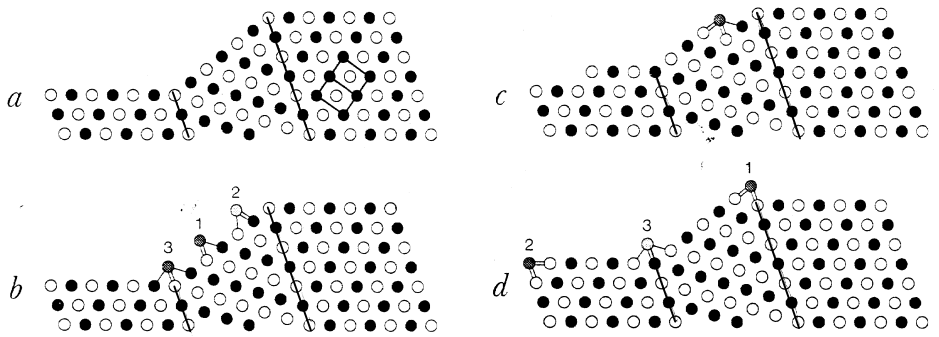

Figure 9. The re-entrant corner growth mechanism of lamellar twinned particles (van de Waal, 1996). Twin boundaries are indicated by solid lines.

probably attached to a re-entrant corner than to the flat {111} surface. The probability is over 60 times higher at 500 °C (Paper VI). Therefore, the re-entrant grooves are the preferential sites for growth of the new layers of fullerene molecules. When a new fullerene molecule has been attached to the re-entrant corner, it creates new favorable sites (5-coordinated) next to it, and a new row of molecules can spread over the re-entrant corner. Molecules attached to the re-entrant corner are surrounded by favorable 5-coordinated sites (Figure 9c), and the new layer is spread until it reaches the end of a crystal or some defect. The shape of the re-entrant corner stays the same and the growth process will start all over again, and produce thin platelets (Figure 9d). A crystal with a single twin will develop into a thin triangular platelet, whereas a crystal with lamellar twins forms hexagonal platelets.

The re-entrant corner growth mechanism proposed for hexagonal plate-like particles was first described for fcc germanium crystals (Hamilton and Seidensticker, 1960; Wagner, 1960). Lamellar-twinned particles have been observed for many fcc metals and a variety of other materials including crystalline C_{60} (Harris, 1995). In fact, hexagonal fullerene particles with planar defects have already been observed in the first images of solid fullerenes by Krätschmer et al. (1990). Harris et al. (1992) suggested that these particles have twins parallel to the large faces {111}. Moreover, the growth mechanism of the lamellar-twinned particles has been discussed in detail by a number of authors

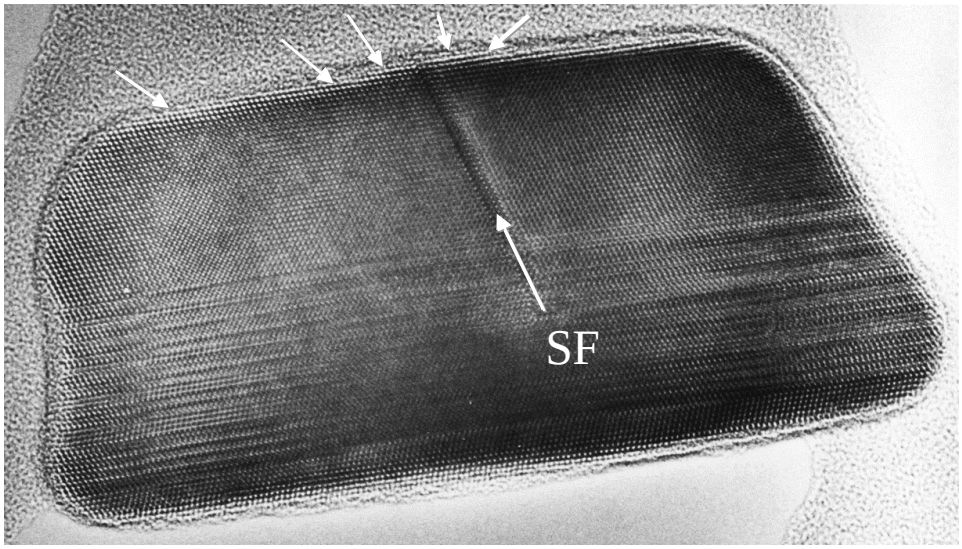

Figure 10. HREM image a lamellar twinned particle "edge on" Note the presence of the stacking fault (SF) and the nucleation of new (111) planes at the stacking fault, indicated as small arrows (Paper III) .

(Ming and Sunagawa, 1988; Ming and Li, 1991; Ming, 1993; Li et al., 1994; van de Waal, 1996).

The thickness growth of the platelets is highly influenced by the occasional presence of defects such as dislocations or stacking faults. An observation of that is shown in Figure 10, where a lamellar particle is imaged "edge on" by HREM. Several (111) layers are observed originating at the surface step caused by a stacking fault which is lying along a different (111) plane. The surface step caused by the stacking fault can act as a step-generation source for crystal growth. Figure 11 illustrates the stacking fault mechanism of crystal growth (Ming et al., 1988; van de Waal, 1996). A sub-step with a height of 1/3 (or 2/3) of the elementary growth layer ($\delta_{(111)}$) is generated by a stacking fault on the (111) surface of an fcc crystal (Figure 11a). A row of molecules will be adsorbed along the sub-step, forming a sub-step with height of 2/3 $\delta_{(111)}$ and a full-step which can quickly grow out (Figure 11b). Subsequently, a new row of molecules will be adsorbed along the new sub-step created, forming an another full-step and a sub-step. This process is repeated, and thus the stacking will operate as a self-perpetuating step source. The coordination numbers in the full-

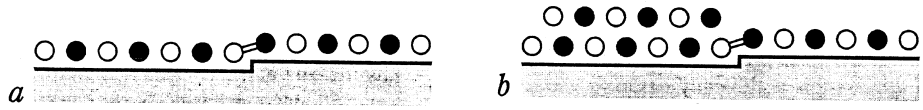

Figure 11. The staking fault mechanism for crystal growth (van de Waal, 1996).

step and the sub-steps are five and four, respectively, while the number is three on a perfect {111} surface, indicating that preferential nucleation in the full-step and the sub-step is very probable. A step generation mechanism from stacking faults has been proposed by Bauser and Strunk (Bauser and Strunk, 1982; Bauser and Strunk, 1984), and it has been discussed in detail by a number of authors (Ming et al., 1988; Jin et al., 1989; Ming, 1993; van de Waal, 1996).

4.3.4 Multiply-twinned particles

The decahedral and icosahedral particles (see Figure 6) are multiply-twinned particles (MTPs) that are often found in the early stages of nucleation and growth of fcc metal crystals in the gas phase and in solutions (see reviews Ajayan and Marks, 1990; Kirkland et al., 1990; Marks, 1994; Hofmeister, 1998). A relatively large number of multiply-twinned particles have been observed for both C_{60} and C_{70} fullerenes (Papers III–V). The multiply-twinned particles adopt preferentially the decahedral or icosahedral shape. They can be considered as five or twenty fcc tetrahedra joined by twin boundaries (Figure 12). A decahedral particle consisting of unstrained fcc tetrahedra cannot be closed: the theoretical angle between two (111) planes is 70.52°, while the wedge angle of the five tetrahedra required for a coherent and continuous decahedral particle is 72°. Nevertheless, the observed decahedral C_{60} and C_{70} particles are continuous, implying that they must be strained (Papers IV and V). Figure 13 shows a HREM image from the center of a decahedral C_{70} particle where five crystals are joined together. The electron diffraction and HREM results of C_{60} and C_{70} particles indicate an orthorhombic expansion along the [110] direction of about 2–3 %, accompanied by an eventual small contraction along the [100] direction. This deformation is sufficient to accommodate the angular deficit in the decahedral particle (Paper V).

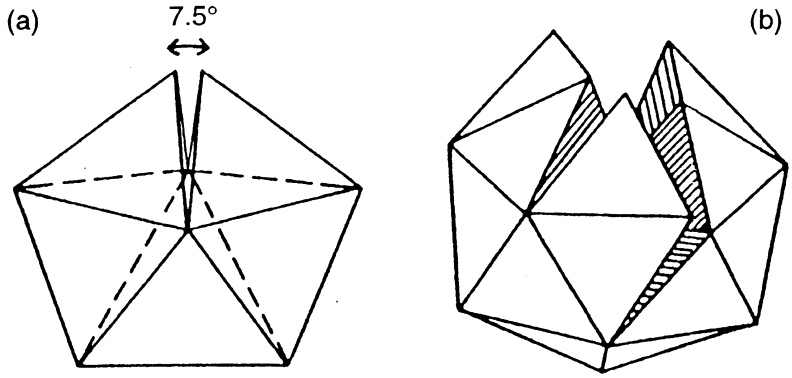

Figure 12. Schematic representation of a) decahedral and b) icosahedral particles consist of five or twenty fcc tetrahedra joined by twin boundaries (Harris, 1995). Particles formed from unstrained fcc tetrahedra have angular defects due to they cannot completely fill the space.

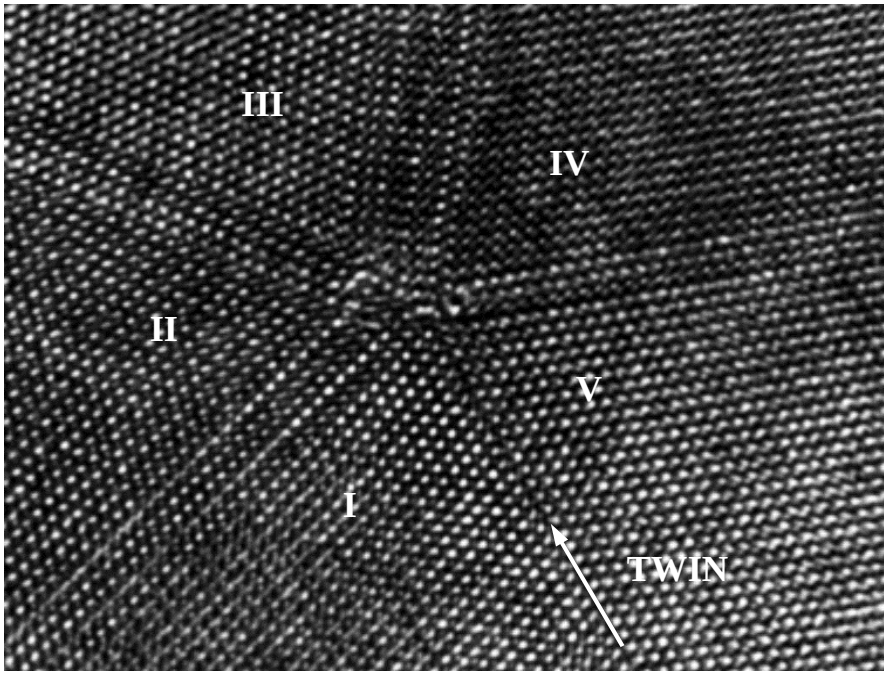

Figure 13. HREM image a multiply twinned particle (decahedral). A twin boundary is marked by a white arrow and the five crystals bonded by twin boundaries are marked by Roman numerals.

Some of the decahedral particles have a modified shape, called Marks' decahedron (see Figure 14) which is the energetically favored shape for small clusters of fcc metals, according to an elastic theory (Marks, 1984) and computer simulations (Cleveland and Landman, 1991). The energy differences between multiply-twinned particles and single crystals are, however, very small, and clusters need not have a single stable structure, but many configurations (Doraiswamy and Marks, 1995). Recent theoretical studies of the relative stability of decahedral, icosahedral or perfect C_{60} fcc clusters demonstrate that the decahedral and fcc structures are the most stable structures for small clusters (more than about 15 molecules) (Doye et al., 1995; Doye et al., 1996; Doye et al., 1997). Once a decahedral cluster (nuclei) is formed, its shape can remain during the crystal growth of the particles. This means that the final particle structure is already formed at the early stages of nucleation and growth. Furthermore, the re-entrant corners of the Marks' decahedron can act as preferred nucleation sites during crystallite growth (Marks, 1984; Marks, 1994), as observed for the lamellar-twinned particles. Each re-entrant twin boundary will act as a permanent source of a new layer of molecules and the lateral growth will proceed toward the center of the edge. The icosahedral particles are probably also formed in a similar way, although the icosahedral shape is favored only for tiny clusters (less than about 15 molecules) (Doye et al., 1997).

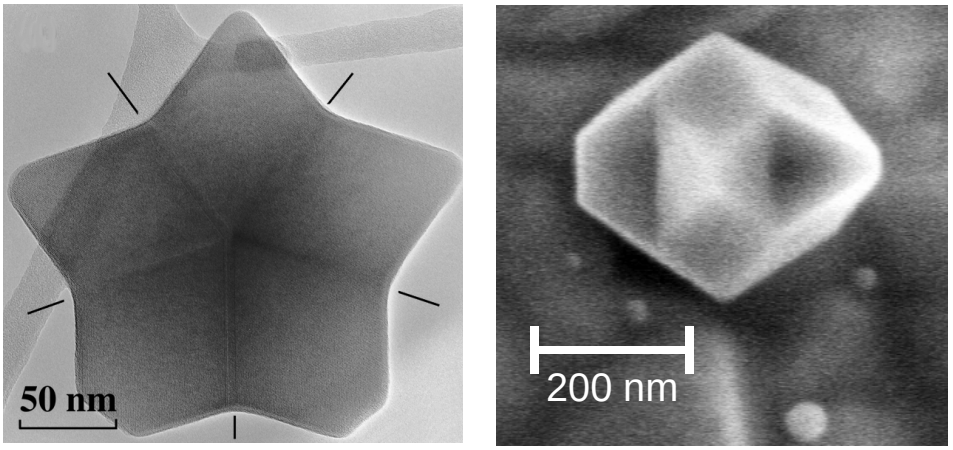

Figure 14. TEM (on left) and SEM (on right) images of fullerene particles with a shape of Marks' decahedron (Paper IV). Twin boundaries of the multiply twinned particle at re-entrant corners are marked by lines in the left image.

No uniform mechanism for the formation of multiply-twinned particles are found in the literature (Ajayan and Marks, 1990; Hofmeister, 1998). The multiply-twinned fullerene particles observed in this study can also be formed during grain growth, particle coalescence and successive twinning (Yagi et al., 1975; Ajayan and Marks, 1990; Hofmeister, 1998). For instance, five or twenty grains in a polycrystalline particle can grow together during grain growth, forming a multiply-twinned particle. In addition, two lamellar twins that are crossed form a region with a local five-fold symmetry. This cross-twinning region may act as an embryo for growth of a decahedral particle (van de Waal, 1996; Hofmeister, 1998).

Decahedral C_{60} particles have previously been observed to form during the growth of thin films by vacuum deposition (Saito et al., 1992; Zhou et al., 1993), by gas-evaporation method (Ohno and Yatsuya, 1998) and large single crystals (millimeter sized) by a sublimation-condensation method in a vacuum (Haluska et al., 1993). To the author's knowledge, icosahedral fullerene particles have not been reported before. However, clusters of C_{60} molecules (13 and 55 molecules) with icosahedral structure have been observed (Martin et al., 1993).

4.3.5 Particle transformation and growth during aerosol synthesis

The growth mechanisms of the lamellar and the multiply-twinned fullerene particles are discussed in the chapters above. In this chapter, the growth mechanisms of the individual particles are connected to the aerosol synthesis processes.

The experiments show that the morphology of the fullerene particles changes from irregular or roughly spherical to clearly crystalline when the processing temperature rises to 500 °C (Papers III–V). The evaporation calculations indicate that a major fraction of fullerene can be vaporized during the synthesis at 500 °C (Paper VI). In addition, the particle size measurements show that fullerene mainly evaporates from particles and subsequently condenses back to the partially evaporated particles during the synthesis (Paper VI). These results indicate that the vaporization of the fullerene particles plays an important role during synthesis of single crystalline particles with well-defined shape during the particle synthesis (Paper VI). A similar particle morphology transformation has been previously observed for volatile metal oxides such as V_2O_5 and MoO_3

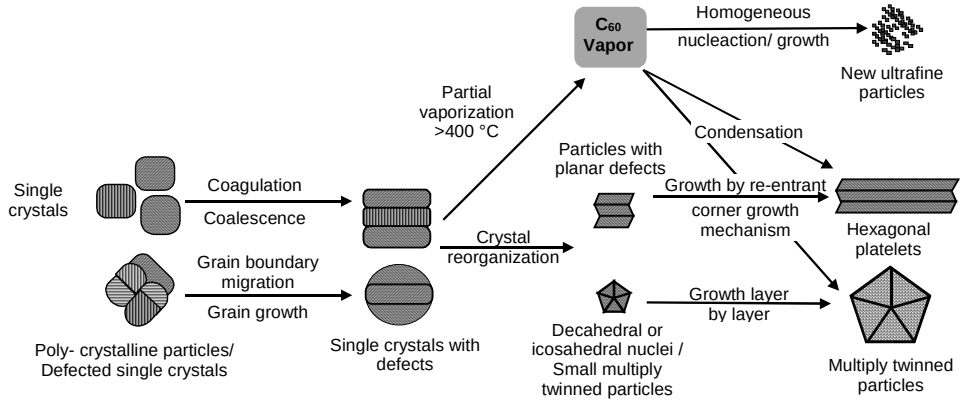

Figure 15. Schematic description of possible mechanisms for the transformation of lamellar and multiply twinned as well as ultrafine fullerene particles during the aerosol processes at 500 °C.

produced via aerosol decomposition (Lyons et al., 1992; Xiong et al., 1992; Kodas and Hampden-Smith, 1999).

The presumable transformation and growth mechanisms for multiply and lamellar-twinned particles occurring during aerosol synthesis are schematically shown in Figure 15. When the fullerene particles enter the heated zone of the reactor, they start to evaporate and the molecules rearrange, e.g. by evaporation/ condensation and surface migration. Simultaneously, particle agglomeration, coalescence and grain growth occur (Paper VI). Finally, decahedral/ icosahedral nuclei or partially vaporized particles with multiple twinning are formed, and subsequently multiply-twinned particles are mainly grown by a layer-by-layer mechanism from the nuclei (Paper IV). The lamellar-twinned particles are grown from partially vaporized particles with planar defects by a re-entrant corner growth mechanism in the direction parallel to the twins and stacking faults (Papers IV–V). Mainly, growth of the multiply and lamellar-twinned particles already occurs in the heated zone. The growth can be accelerated by condensation at the reactor exit when the aerosol cools. In addition, new ultrafine particles can be formed via homogeneous nucleation and condensation.

The growth of the particles with well-defined crystal habit is often promoted by defects, such as twins and stacking faults (Papers IV–VI). Defects can be formed during grain growth and particle agglomeration and coalescence

(McGinn et al., 1982b; McGinn et al., 1982a; Mumaw and Haugh, 1986; Harris, 1995). Particles are mainly polycrystalline up to temperatures of 400 °C, indicating that grain growth is probably the main mechanism to introduce defects. Impurities in the particles can also form defects during particle crystallization. Furthermore, defects frequently occur in large single fullerene crystals even if they have grown very slowly from the gas phase. The microstructure of these fullerene crystals is very similar to those of fcc metals and alloys with a low stacking fault energy (Muto et al., 1992; Van Tendeloo et al., 1992).

At 600 °C, the particles have a less distinct crystal habit when produced in the controlled conditions (Paper VI). The transformation and growth mechanisms of fullerene particles are shown in Figure 16 in Paper VI. The fullerene particles are vaporized almost completely in the heated zone. Subsequently, fullerene vapor condenses onto the surfaces of the residual particles and also forms new ultrafine particles via homogeneous nucleation and condensation at the reactor outlet where the carrier gas cools down. Clearly faceted particles are not formed during fast cooling. In addition, the crystal structure and the surface morphology may be destroyed thermally at higher temperatures. Furthermore, the defects that promote crystal growth may migrate along the crystal and disappear at higher temperatures.

5. Conclusions

The primary objectives of this thesis were to develop routes for the production of nanostructured, ultrafine fullerene particles and to understand fullerene particle formation and crystallization mechanisms during the aerosol synthesis. When developing new applications for fullerene-based nanostructured materials, the production method techniques of nanostructured fullerene particles need to be developed. The nanostructured, ultrafine fullerene particles were produced by vapor condensation and by aerosol droplet drying and crystallization methods in tubular flow reactors. The formation and crystallization mechanisms were studied using aerosol measurement techniques (DMA, LPI) and electron microscopy (SEM, TEM and HREM). The production conditions and the vaporization of fullerene particles during the synthesis were evaluated using computational fluid dynamics and evaporation calculations. In addition, a high-performance liquid-chromatography method was utilized to study whether it is possible to separate different fullerenes during aerosol processes.

The study demonstrated that ultrafine (30–60 nm) fullerene particles can be generated by vapor condensation in a continuous flow reactor. The size of the fullerene particles can be controlled by changing the reactor temperature. The particles are spherical, solid and polycrystalline at processing temperatures of 500 °C and above.

The larger fullerene particles, around 100 nm in size, were produced by using the aerosol droplet drying and crystallization method starting from fullerene toluene solution. The particles are roughly spherical, having pores and voids, and are nanocrystalline when produced at low reactor operating temperatures (20–200 °C). At higher temperatures of up to 400 °C, the particles are denser and mostly polycrystalline. The crystallinity of the fullerene particles can be controlled by varying the reactor operating temperature during the aerosol droplet drying synthesis.

Fullerene particles with a clear faceted shape were observed at processing temperatures of 500 °C and above. The most common shapes among perfectly faceted particles were hexagonal plate-like, decahedral and icosahedral shapes. Electron microscopy revealed that the plate-like particles are lamellar twinned whereas the decahedral and icosahedral particles are multiply twinned. The

lamellar-twinned particles are probably grown rapidly on the side-faces in the direction parallel to the twins by a re-entrant corner growth mechanism, while the large close-packed {111} faces grow relatively slowly. No uniform mechanism was found for the formation of multiply-twinned particles. The multiply-twinned particles are probably grown layer-by-layer around the exiting decahedral and icosahedral nuclei, which are stable structures for small fullerene clusters. Furthermore, the multiply-twinned particles can be formed during grain growth from polycrystalline particles, particle coalescence and successive twinning.

The growth of the particles with well-defined crystal habit is often promoted by defects, such as twins and stacking faults. Furthermore, the vaporization of fullerene particles and the fullerene vapor play an important role during the formation and growth of particles with a clearly faceted shape. For multiply and lamellar twinned particles, following particle formation and crystallization phenomena during the aerosol synthesis fullerene particle are proposed. At 500 °C, during particle vaporization in the reactor, decahedral/icosahedral nuclei or partially vaporized particles with multiple twinning are formed, and, subsequently, the multiply-twinned particles are probably grown by a layer-by-layer mechanism. Similarly, the lamellar-twinned particles are grown from partially vaporized particles with planar defects by a re-entrant corner growth mechanism in the direction parallel to the twins and stacking faults. The growth of the particles mainly occurs already in the heated zone of the reactor. The growth can be accelerated by condensation at the reactor exit when the aerosol cools. At 600 °C, the particles have a less distinct crystal habit. The fullerene particles are vaporized almost completely in the heated zone. Subsequently, fullerene vapor condenses onto the surfaces of the residual particles. In addition at high temperatures (500–600 °C), new ultrafine particles are formed via homogeneous nucleation and condensation from fullerene vapor at the reactor outlet where the carrier gas cools down.

Computational fluid dynamics calculations show that with a careful reactor design, uniform conditions with respect to temperature and flow profiles, as well as residence times in the heated zone, can be achieved in a small tubular aerosol reactor using a low aerosol flow rate. The uniform reactor conditions and residence times of few seconds at least for particle formation and crystallization indicate that particles with relatively homogeneous crystallinity

and morphology can be produced. Experiments show that almost all of the particles are hexagonal platelets produced in particular processing conditions at 500 °C.

The high performance liquid chromatography results from size-classified samples indicate that only minor fractionation occurs during the synthesis of mixed fullerene particles, due to the small difference of partial vapor pressures. Furthermore, C_{60} and C_{70} molecules are fully miscible in the crystals of the particles, forming alloys of fullerenes. The results show that it is difficult to separate different fullerenes by aerosol droplet drying, vaporization of fullerenes and subsequent vapor condensation when starting from C_{60}–C_{70} solution droplets.

In summary, ultrafine, nanostructured fullerene particles can be produced by aerosol processing methods. Particle size can be controlled from 20 nm to 300 nm and crystallinity from nanocrystalline to single crystal. Furthermore, the defects such as stacking faults and twins as well as vaporization of the fullerene particles play an important role during the crystal growth of the fullerene particles with distinct crystal habit. The synthesis method can also be extended to process, for instance, fullerene metal composites and compounds. For possible applications, fullerene particles produced in this study can be used in medical applications for visualization *in vivo* of the lymphatic system, and as a carrier material for drugs, isotopes and antibodies.

The formation mechanisms of multiply-twinned particles are not clear as yet. Further studies are needed to clarify the formation mechanisms of multiply-twinned particles. However, the formation of multiply-twinned particles could be a chance phenomenon, indicating that particles are only be formed occasionally. Finally, it will be interesting to develop aerosol-processing routes for the production of carbon nanotubes, which have very interesting properties and possible applications.

References

Ahn, J. S., Suzuki, K., Iwasa, Y., Otsuka, N. and Mitani, T. 1998. Photoluminescence of confined excitons in nanoscale C_{60} clusters. Journal of Luminescence, Vol. 77&78, p. 201–205.

Ajayan, P. M. and Marks, L. D. 1990. Phase instabilities in small particles. Phase Transitions, Vol. 24–26, p. 229–258.

Amelinckx, S., Van Dyck, D., Van Landuyt, J. and Van Tendeloo, G. 1997. Handbook of microscopy: applications in materials science, solid-state physics and chemistry. Methods I. Weinheim, VCH Verlagsgesellschaft mbH. 536 p.

Andrievsky, G. V., Kosevich, M. V., Vovk, O. M., Shelkovsky, V. S. and Vashchenko, L. A. 1995. On the production of an colloidal solution of fullerene fullerenes. Journal of the Chemical Society, Chemical Communications, p. 1281–1282.

Ashcroft, N. W. and Mermin, N. D. 1976. Solid state physics. Philadelphia, CBS Publishing Asia Ltd. 826 p.

Baba, M. S., Narasimhan, T. S. L., Balasubramanian, R., Sivaraman, N. and Mathews, C. K. 1994. Studies on the thermodynamics of the C_{60} and C_{70} binary system. Journal of Physical Chemistry, Vol. 98, p. 1333–1340.

Ball, P. and Garwin, L. 1992. Science at the atomic scale. Nature, Vol. 355, p. 761–766.

Bauser, E. and Strunk, H. 1982. Dislocations as growth step sources in solution growth and their influence on interface structures. Thin Solid Films, Vol. 93, p. 185–194.

Bauser, E. and Strunk, H. P. 1984. Microscopic growth mechanisms of semiconductors: experiments and models. Journal of Crystal Growth, Vol. 69, p. 561–580.

Berner, A. 1984. Desing principles of the Aeras low-pressure impactor. In: Liu, B. Y. H., Pui, D. Y. H. and Fissan, H. Aerosols: Science, technology and industrial applications of airborne particles. New York, Elsevier, p. 139–142.

Berner, A. and Lürzer, C. 1980. Mass size distributions of traffic aerosols at Vienna. Journal of Physical Chemistry, Vol. 84, p. 2079–2083.

Buntar, V. and Weber, H. W. 1996. Magnetic properties of fullerene superconductors. Superconducting Science and Technology, Vol. 9, p. 599–615.

Ceolin, R., Michaud, F., Toscani, S., Agafonov, V., Tamarit, J. L., Dworkin, A. and Szwarc, H. 1997. Crystals of C_{60} solvates. Electrochemical Society Proceedings, Vol. 97–42 (Recent Advances in the Chemistry and Physics of Fullerenes and Related Materials, Vol. 5), p. 373–381.

Cleveland, C. L. and Landman, U. 1991. The energetics and structure of nickel clusters: Size dependence. Journal of Chemical Physics, Vol. 94, p. 7376–7396.

Doraiswamy, N. and Marks, L. D. 1995. Preferred structures in small particles. Philosophical Magazine B, Vol. 71, p. 291–310.

Doye, J. P. K., Dullweber, A. and Wales, D. J. 1996. The structure of $(C_{60})_N$ clusters. Chemical Physics Letters, Vol. 262, p. 167–174.

Doye, J. P. K., Dullweber, A. and Wales, D. J. 1997. Structural predictions for $(C_{60})_N$ clusters with an all-atom potential. Chemical Physics Letters, Vol. 269, p. 408–412.

Doye, J. P. K., Wales, D. J. and Berry, R. S. 1995. The effect of the range of the potential on the structures of clusters. Journal of Chemical Physics, Vol. 103, p. 4234–4249.

Dresselhaus, M. S., Dresselhaus, G. and Eklund, P. C. 1993. Fullerenes. Journal of Materials Research, Vol. 8, p. 2054–2097.

Dresselhaus, M. S., Dresselhaus, G. and Eklund, P. C. 1996. Science of fullerenes and carbon nanotubes. San Diego, Academic Press. 965 p.

Edelstein, A. S. and Cammarata, R. C., Eds. 1996. Nanomaterials: synthesis, properties and applications. Bristol, Institute of Physics Publishing. 596 p.

El-Shall, M. S. and Edelstein, A. S. 1996. Formation of clusters and nanoparticles from supersaturated vapor and selected properties. In: Edelstein, A. S. and Cammarata, R. C. Nanomaterials: synthesis, properties and applications. Bristol, Institute of Physics Publishing, p. 13–54.

Fischer, J. E. 1993. Structure and dynamics of solid C_{60} and its intercalation compounds. Materials Science and Engineering, B, Vol. 19, p. 90–99.

Flagan, R. C. and Seinfeld, J. H. 1988. Fundamentals of air pollution engineering. Englewood Cliffs, Prentice Hall. 542 p.

Fleming, R. M., Hassen, B., Siegrist, T., Kortan, A. R., Tycko, R., Marsh, P. and Haddon, R. C. 1992. Crystalline fullerenes. In: Hammond, G. S. and Kuck, V. J. Fullerenes: synthesis, properties, and chemistry of large carbon clusters. Washington, American Chemical Society, p. 25–39.

Fleming, R. M., Kortan, A. R., Hassen, B., Siegrist, T., Thiel, F. A., Marsh, P., Haddon, R. C., Tycko, R., Dabbagh, G., Kaplan, M. L. and Mujsce, A. M. 1991a. Pseudotenfold symmetry in pentane-solvated C_{60} and C_{70}. Physical Review B, Vol. 44, p. 888–891.

Fleming, R. M., Siegrist, T., Marsh, P., Hassen, B., Kortan, A. R., Murphy, D. W., Haddon, R. C., Tycko, R., Dabbagh, G., Mujsce, A. M., Kortan, A. R. and Zahurak, S. M. 1991b. Diffraction symmetry in crystalline, close-packed C_{60}. Materials Research Society Symposium Proceedings, Vol. 206, p. 691–695.

Fujitsuka, M., Kasai, H., Masuhara, A., Okada, S., Oikawa, H., Nakanishi, H., Watanabe, A. and Ito, O. 1997. Laser flash photolysis study on photochemical and photophysical properties of C_{60} fine particle. Chemistry Letters, p. 1211–1212.

Gao, M. and Zhang, H. 1996. Preparation of an amorphous fullerene film. Physics Letters A, Vol. 213, p. 203–206.

Gleiter, H. 1989. Nanocrystalline materials. Progress in Materials Science, Vol. 33, p. 223–315.

Gleiter, H. 1992. Materials with ultrafine microstructures: retrospectives and perspectives. Nanostructured Materials, Vol. 1, p. 1–19.

Gurav, A. S., Duan, Z., Wang, L., Hampden-Smith, M. J. and Kodas, T. T. 1993a. Synthesis of fullerene-rhodium nanocomposites via aerosol decomposition. Chemistry of Materials, Vol. 5, p. 214–216.

Gurav, A. S., Kodas, T., Pluym, T. and Xiong, Y. 1993b. Aerosol processing of materials. Aerosol Science and Technology, Vol. 19, p. 411–452.

Gurav, A. S., Kodas, T. T., Wang, L.-M., Kauppinen, E. I. and Joutsensaari, J. 1994. Gas-phase particle size distributions during vapor phase condensation of fullerenes. Nanostructured Materials, Vol. 4, p. 491–496.

Gurav, A. S., Pluym, T., Kodas, T. T. and Pratsinis, S. E. 1996. Grain growth and densification in palladium oxide particles during spray pyrolysis. Chemical Engineering Communications, Vol. 151, p. 211–226.

Haddon, R. C., Perel, A. S., Morris, R. C., Palstra, T. T. M., Hebard, A. F. and Fleming, R. M. 1995. C_{60} thin film transistor. Applied Physics Letters, Vol. 67, p. 121–123.

Hagen, M. H. J., Meijer, E. J., Mooij, G. C. A. M., Frenkel, D. and Lekkerkekker, H. N. W. 1993. Does C_{60} have a liquid phase? Nature, Vol. 365, p. 425–426.

Haluska, M., Kuzmany, H., Vybornov, M., Rogl, P. and Fejdi, P. 1993. A double-temperature-gradient technique for the growth of single-crystal fullerites from the vapor phase. Applied Physics A, Vol. 56, p. 161–167.

Hamilton, D. R. and Seidensticker, R. G. 1960. Propagation mechanism of germanium dentrides. Journal of Applied Physics, Vol. 31, p. 1165–1168.

Harris, P. J. F. 1995. Growth and structure of supported metal catalyst particles. International Materials Reviews, Vol. 40, p. 97–115.

Harris, P. J. F., Douthwaite, R. E., Stephens, A. H. H. and Turner, J. F. C. 1992. The structure and growth of C_{60} platelets. Chemical Physics Letters, Vol. 199, p. 631–634.

Hartman, P. and Perdok, W. G. 1955a. On the relations between structure and morphology of Crystals. I. Acta Crystallographica, Vol. 8, p. 49–52.

Hartman, P. and Perdok, W. G. 1955b. On the relations between structure and morphology of Crystals. II. Acta Crystallographica, Vol. 8, p. 521–524.

Hartman, P. and Perdok, W. G. 1955c. On the relations between structure and morphology of Crystals. III. Acta Crystallographica, Vol. 8, p. 525–529.

Hebard, A. F., Haddon, R. C., Fleming, R. M. and Kortan, A. R. 1991a. Deposition and characterization of fullerene films. Applied Physics Letters, Vol. 59, p. 2109–2111.

Hebard, A. F., Rosseinsky, M. J., Haddon, R. C., Murphy, D. W., Glamur, S. H., Palstra, T. T. M., Ramirez, A. P. and Kortan, A. R. 1991b. Superconductivity at 18 K in potassium-doped C_{60}. Nature, Vol. 350, p. 600–601.

Hillamo, R. E. and Kauppinen, E. I. 1991. On the performance of the Berner low pressure impactor. Aerosol Science and Technology, Vol. 14, p. 33–47.

Hinds, W. C. 1999. Aerosol technology: properties, behavior and measurement of airborne particles, Second edition. New York, John Wiley & Sons. 483 p.

Hofmeister, H. 1998. Forty years study of fivefold twinned structures in small particles and thin films. Crystal Research and Technology, Vol. 33, p. 3–25.

Howard, J. B., McKinnon, J. T., Johnson, M. E., Makarovsky, Y. and Latleur, A. L. 1992. Production of C_{60} and C_{70} fullerenes in benzene-oxygen flames. Journal of Physical Chemistry, Vol. 96, p. 6657–6662.

Huffman, D. R. 1996. Synthesis, structure, and properties of fullerenes. In: Edelstein, A. S. and Cammarata, R. C. Nanomaterials: synthesis, properties and applications. Bristol, Institute of Physics Publishing, p. 477–494.

Ichinose, N., Ozaki, Y. and Karsu, S. 1992. Superfine particle technology. London, Springer-Verlag. 223 p.

Ito, K., Ogawa, K. and Ishida, Y. 1998. Preferred orientations in compression deformed and annealed polycrystalline C_{60}. Materials Transactions, JIM, Vol. 39, p. 648–651.

Janda, P., Krieg, T. and Dunsch, L. 1998. Nanostructuring of high ordered C_{60} films by charge transfer. Advanced Materials, Vol. 10, p. 1434–1438.

Jensen, H. and Sorensen, G. 1996. Ion bombardment of the nano-particle coatings. Surface and Coatings Technology, Vol. 84, p. 500–505.

Jin, J.-M., Ming, N. and Chernov, A. A. 1989. The growth mechanism and kinetics on stacking fault reconsidered. Journal of Crystal Growth, Vol. 98, p. 341–344.

Joutsensaari, J. and Kauppinen, E. I. 1997. Production of nanostructured iron oxide particles via aerosol decomposition. Materials Research Society Symposium Proceedings, Vol. 457, p. 75–80.

Kauppinen, E. I. and Pakkanen, T. A. 1990. Coal combustion aerosols: a field study. Environmental Science and Technology, Vol. 24, p. 1811–1818.

Kingery, W. D., Bowen, H. K. and Uhlmann, D. R. 1976. Introduction to ceramics, Second edition. New York, John Wiley & Sons. 1032 p.

Kirkland, A. I., Edwards, P. P., Jefferson, D. A. and Duff, D. G. 1990. The structure, characterization, and evolution of colloidal metals. Annual Reports on the Progress of Chemistry (Sect. C), Vol. 87, p. 247–304.

Kniaz, K., Fischer, J. E., Girifalco, L. A., McGhie, A. R., Strongin, R. M. and III, A. B. S. 1995. Fullerene alloys. Solid State Communications, Vol. 96, p. 739–743.

Knutson, E. O. and Whitby, K. T. 1975. Aerosol classification by electric mobility: apparatus, theory and applications. Journal of Aerosol Science, Vol. 6, p. 443–451.

Kodas, T. T. 1989. Generation of complex metal oxides by aerosol processes: superconducting ceramic particles and films. Angewandte Chemie International Edition, Vol. 28, p. 794–807.

Kodas, T. T. and Hampden-Smith, M. J. 1999. Aerosol processing of materials. New York, Wiley-VCH. 680 p.

Kolari, P. J., Maaranen, P., Kauppinen, E., Joutsensaari, J., Jauhiainen, K., Pelkonen, K. and Rannikko, S. 1995. Nanoparticles for visualization, contrast enhancement and drug delivery in lymphatic targetting. Journal of Aerosol Science, Vol. 26, p. S225–S226.

Kolari, P. J., Maaranen, P., Kauppinen, E., Joutsensaari, J., Jauhiainen, K., Pelkonen, K. and Rannikko, S. 1996. Nanoparticles in biomedical applications: experiments with activated carbon, fullerene and iron oxide. Medical & Biological Engineering & Computing, Vol. 34 S1, p. 153–154.

Krakow, W., Rivera, N. M., Roy, R. A., Ruoff, R. S. and Cuomo, J. J. 1993. The growth of crystalline vapor deposited carbon-60 thin films. Applied Physics A, Vol. 56, p. 185–192.

Kroto, H. W., Heath, J. R., O´Brien, S. C., Curl, R. F. and Smalley, R. E. 1985. C_{60}: Buckminsterfullerene. Nature, Vol. 318, p. 162–163.

Kruis, F. E., Fissan, H. and Peled, A. 1998. Synthesis of nanoparticles in the gas phase for electrical, optical and magnetic applications – a review. Journal of Aerosol Science, Vol. 29, p. 511–535.

Krätschmer, W., Lamb, L. D., Fostiropoulos, K. and Huffman, D. R. 1990. Solid C_{60}: a new form of carbon. Nature, Vol. 347, p. 354–358.

Li, H., Peng, X.-D. and Ming, N. 1994. Re-entrant corner mechanism of fcc crystal growth of A-type twin lamella: the Monte-Carlo simulation approach. Journal of Crystal Growth, Vol. 139, p. 129–133.

Li, Y. Z., Patrin, J. C., Chander, M., Weaver, J. H., Chibante, L. P. F. and Smalley, R. E. 1991. Ordered overlayers of C_{60} on GaAs(110) studied with scanning tunneling microscopy. Science, Vol. 252, p. 547–548.

Liu, J. Z., Dykes, J. W., Lan, M. D., Klavins, P., Shelton, R. N. and Olmstead, M. M. 1993. Vapor transport growth of C_{60} crystals. Applied Physics Letters, Vol. 62, p. 531–532.

Liu, X. Y. and Bennema, P. 1996. Prediction of the growth morphology of crystals. Journal of Crystal Growth, Vol. 166, p. 117–123.

Lyons, S. W., Wang, L. M. and Kodas, T. T. 1992. Nanophase oxide formation by intraparticle reaction. Nanostructured Materials, Vol. 1, p. 283–291.

Lüthi, R., Haefke, H., Meyer, E., Howard, L., Land, H.-P., Gerth, G. and Güntherodt, H.-J. 1994a. Frictional and atomic-scale study of C_{60} thin films by scanning force microscopy. Zeitschrift für Physik B, Vol. 95, p. 1–3.

Lüthi, R., Meyer, E., Haefke, H., Howard, L., Gutmannsbauer, W. and Güntherodt, H.-J. 1994b. Sled-type motion on the nanometer scale: determination of dissipation and cohesive energies of C_{60}. Science, Vol. 266, p. 1979–1981.

Marks, L. D. 1984. Surface structure and energetics of multiply twinned particles. Philosophical Magazine A, Vol. 49, p. 81–93.

Marks, L. D. 1994. Experimental studies of small particle structures. Reports on Progress in Physics, Vol. 57, p. 603–649.

Martin, T. P., Näher, U., Schaber, H. and Zimmermann, U. 1993. Clusters of fullerene molecules. Physical Review B, Vol. 70, p. 3079–3082.

McGinn, J. T., Greenhut, V. A. and Tsukalakos, T. 1982a. Formation of fault structures during coalescence and growth of gold particles in a fused silica matrix - I. Acta metallurgica, Vol. 30, p. 2093–2102.

McGinn, J. T., Greenhut, V. A. and Tsukalakos, T. 1982b. A mechanism for fault formation in fine particles and implications for theories of annealing twins in F.C.C. metals - II. Acta metallurgica, Vol. 30, p. 2103–2110.

Meng, R. L., Ramirez, D., Jing, X., Chow, P. C., Diaz, C., Matsuishi, K., Moss, S. C., Hor, P. H. and Chu, C. W. 1991. Growth of large, defect-free pure C_{60} single crystals. Applied Physics Letters, Vol. 59, p. 3402–3403.

Messing, G. L., Zhang, S.-C. and Jayanthi, G. V. 1993. Ceramic powder synthesis by spray pyrolysis. Journal of the American Ceramic Society, Vol. 76, p. 2704–2726.

Milani, P. and Manfredini, M. 1996. Surface periodic structures induced by pulced laser irradiation of fullerite. Applied Physics Letters, Vol. 68, p. 1769–1771.

Ming, N. 1993. Defect mechanisms of the crystal growth and their kinetics. Journal of Crystal Growth, Vol. 128, p. 104–112.

Ming, N. and Li, H. 1991. Twin lamella mechanism of fcc crystal growth: the Monte-Carlo simulation approach. Journal of Crystal Growth, Vol. 115, p. 199–202.

Ming, N. and Sunagawa, I. 1988. Twin lamellae as possible self-perpetuating step source. Journal of Crystal Growth, Vol. 87, p. 13–17.

Ming, N., Tsukamoto, K., Sunagawa, I. and Chernov, A. A. 1988. Stacking faults as self-perpetuating step sources. Journal of Crystal Growth, Vol. 91, p. 11–19.

Mumaw, C. T. and Haugh, E. F. 1986. Silver halide precipitation coalescence processes. Journal of Imaging Science, Vol. 30, p. 198–209.

Muto, S., Van Tendeloo, G. and Amelinckx, S. 1992. High-resolution electron microscopy of structural defects in crystalline C_{60} and C_{70}. Philosophical Magazine B, Vol. 67, p. 443–463.

Ohno, T. and Yatsuya, S. 1998. Growth of fullerene nanoparticles prepared by the gas-evaporation technique. Journal of Materials Science, Vol. 33, p. 5843–5847.

Piacente, V., Gigli, G., Scardala, P., Giustini, A. and Bardi, G. 1996. Vapor pressure of C_{70} fullerene. Journal of Physical Chemistry, Vol. 100, p. 9815–9819.

Piacente, V., Gigli, G., Scardala, P., Giustini, A. and Ferro, D. 1995. Vapor pressure of C_{60} buckminsterfullerene. Journal of Physical Chemistry, Vol. 99, p. 14052–14057.

Pratsinis, S. E. 1998. Flame aerosol synthesis of ceramic powders. Progress in Energy Combustion Science, Vol. 24, p. 197–219.

Pratsinis, S. E. and Kodas, T. T. 1993. Manufacturing of materials by aerosol processes. In: Willeke, K. and Baron, P. Aerosol measurement: principles, techniques and applications. New York, Van Nostrand Reinhold, p. 721–746.

Rao, C. N. R., Seshadri, R., Govindaraj, A. and Sen, R. 1995. Fullerenes, nanotubes, onions and related carbon structures. Materials Science and Engineering, R, Vol. 15, p. 209–262.

Reischl, G. P. 1991. Measurement of ambient aerosols by the different mobility analyzer method: concepts and realization criteria for the size range between 2 and 500 nm. Aerosol Science and Technology, Vol. 14, p. 5–24.

Richter, A., Ries, R., Szulzewsky, K., Pietzak, B. and Smith, R. 1997. The growth mechanisms and morphology of C_{60} films on different substrates. Surface Science, Vol. 394, p. 201–220.

Rogers, R. R. and Yau, M. K. 1989. A short course in cloud physics, Third edition. Oxford, Pergamon Press. 293 p.

Ruoff, R. S., Tse, D. S., Malhotra, R. and Lorents, D. C. 1993. Solubility of C_{60} in a variety organic solvents. Journal of Physical Chemistry, Vol. 97, p. 3379–3383.

Saab, A. P., Laub, M., Srdanov, V. I. and Stucky, G. D. 1998. Oxidized thin films of C_{60}: a new humidity-sensing material. Advanced Materials, Vol. 10, p. 462–465.

Saito, Y., Ishikawa, Y., Ohshita, A., Shinohara, H. and Nagashima, H. 1992. Fivefold twinned C_{60} crystals grown by vacuum deposition. Physical Review B, Vol. 46, p. 1846–1848.

Saito, Y., Yoshikawa, T., Ishikawa, Y., Nagashima, H. and Shinohara, H. 1993. Electron microscopy of fullerene thin films grown on solid surfaces. Materials Science and Engineering, B, Vol. 19, p. 18–24.

Scheibel, H. G. and Porstendörfer, J. 1983. Generation of monodisperse Ag- and NaCl-aerosols with particle diameters between 2 and 300 nm. Journal of Aerosol Science, Vol. 14, p. 133–126.

Scrivens, W. A. and Tour, J. M. 1994. Synthesis of ^{14}C-labeled C_{60}, its suspension in water, and its uptake by human karatinocytes. Journal of the American Chemical Society, Vol. 116, p. 4517–4518.

Seker, C., Dnanasekaran, R. and Subramanian, C. 1996. Effect of molecular rotation on vapor phase nucleation: C_{60} and C_{70}. Fullerene Science and Technology, Vol. 4, p. 553–563.

Siegel, R. W. 1993. Nanophase materials: synthesis, structure, and properties. In: Fujita, F. E. Physics of new materials. Berlin, Springer-Verlag, p. 65–105.

Sivaraman, N., Dhamodaren, R., Kaliappan, I., Srinivasan, T. G., Vasudeva Rao, P. R. and Mathews, C. K. 1992. Solubility of C_{60} in organic solvents. Journal of Organic Chemistry, Vol. 27, p. 6077–6079.

Smalley, R. E. and Yakobson, B. I. 1998. The future of the fullerenes. Solid State Communications, Vol. 107, p. 597–606.

Suryanarayana, C. 1995. Nanocrystalline materials. International Materials Reviews, Vol. 40, p. 41–64.

Tada, T. and Kanayama, T. 1996. Nanolithography using fullerene films as an electron beam resist. Japan Journal of Applied Physics, Part 2, Vol. 35, p. L63–L65.

Talyzin, A. V., Ratnikov, V. V. and Syrnikov, P. P. 1996. Growth of fullerene single crystals from a benzene solution. Physics of the Solid State, Vol. 38, p. 1248–1251.

Tanigaki, K. 1995. Nano-technology and science expected from fullerenes. Optoelectronics – Devices and Technologies, Vol. 10, p. 231–246.

Tanigaki, K., Kuroshima, S., Fujita, J. and Ebbesen, T. W. 1993. Crystal growth of C_{60} thin films on layered substrates. Applied Physics Letters, Vol. 63, p. 2351–2353.

Uyeda, R. 1991. Studies on ultrafine particles in Japan. Methods of preparation and technological applications. Progress in Materials Science, Vol. 35, p. 1–96.

Wagner, R. S. 1960. On the growth of germanium dendrites. Acta metallurgica, Vol. 8, p. 57–60.

Van Cleempoel, A., Gijbels, R., Zhu, D., Claeys, M., Richter, H. and Fonseca, A. 1996. Quantitative determination of C_{60} and C_{70} in soot extracts by high performance liquid chromatography and mass spectrometer characterization. Fullerene Science and Technology, Vol. 4, p. 1001–1017.

van de Waal, B. W. 1996. Cross-twinning model of fcc crystal growth. Journal of Crystal Growth, Vol. 158, p. 153–165.

Van Tendeloo, G., Amelinckx, S., De Boer, J. L., Van Smaalen, S., Verheijen, M. A., Meekes, H. and Meijer, G. 1993. Structural phase transitions in C_{70}. Euraphysics Letters, Vol. 21, p. 329–334.

Van Tendeloo, G., Van Heurck, C., Van Landuyt, J., Amelinckx, S., Verheijen, M. A., van Loosdrecht, P. H. M. and Meijer, G. 1992. Phase transitions in C_{60} and related microstructures: A study by electron diffraction and electron microscopy. Journal of Physical Chemistry, Vol. 96, p. 7424–7430.

Wang, S. C. and Flagan, R. C. 1990. Scanning electrical mobility spectrometer. Aerosol Science and Technology, Vol. 13, p. 230–240.

Verheijen, M. A., Meekes, H., Meijer, G., Bennema, P., De Boer, J. L., Van Smaalen, S., Van Tendeloo, G., Amelinckx, S., Muto, S. and Van Landuyt, J. 1992a. The structure of different phases of pure C_{70} crystals. Chemical Physics, Vol. 166, p. 287–297.

Verheijen, M. A., Meekes, H., Meijer, G., Raas, E. and Bennema, P. 1992b. Growth and morphology of C_{60} crystals. Chemical Physics Letters, Vol. 191, p. 339–344.

Verheijen, M. A., Van Enckevort, W. J. P. and Meijer, G. 1993. Growth phenomena on C_{60} crystals. Chemical Physics Letters, Vol. 214, p. 72–80.

Williams, D. B. and Carter, C. B. 1996. Transmission electron microscopy: a textbook for materials science. New York, Plenum Press. 729 p.

Wragg, J. L., Chamberlain, J. E., White, H. W., Krätschmer, W. and Huffman, D. R. 1990. Scanning tunnelling microscopy of solid C_{60}/C_{70}. Nature, Vol. 348, p. 623–624.

Xiong, Y., Lyons, S. W. and Kodas, T. T. 1992. Volatile metal oxide evaporation during aerosol decomposition. Journal of the American Ceramic Society, Vol. 78, p. 2490–2496.

Yagi, K., Takayanagi, K., Kogayashi, K. and Hohjo, G. 1975. In-situ observations of the growth processes of multiply twinned particles. Journal of Crystal Growth, Vol. 28, p. 117–124.

Yanagi, H. and Sasaki, T. 1994. Epitaxial growth of C_{60} and KI(001) surface. Applied Physics Letters, Vol. 65, p. 1222–1223.

Yao, J., Zou, Y., He, D. and Chen, G. 1997. Electrical conductivity of sulfur-doped C_{60} films. Materials Letters, Vol. 33, p. 27–30.

Ying, Q., Marecek, J. and Chu, B. 1994. Slow aggregation of buckminsterfullerene (C_{60}) in benzene solution. Chemical Physics Letters, Vol. 219, p. 214–218.

Yosida, Y., Arai, T. and Suematsu, H. 1992. Growth of face-centered-cubic single crystals of C_{60} from boiling benzene. Applied Physics Letters, Vol. 61, p. 1043–1044.

Zhou, W. L., Zhao, W., Fung, K. K., Chen, L. Q. and Zhang, Z. B. 1993. Microstructures of C_{60} textured thin film. Physica C, Vol. 214, p. 19–24.

Published by

Vuorimiehentie 5, P.O.Box 2000, FIN-02044 VTT, Finland
Phone internat. +358 9 4561
Fax +358 9 456 4374

Series title, number and report code of publication

VTT Publications 400
VTT–PUBS–400

Author(s)
Joutsensaari, Jorma

Title

Aerosol synthesis of nanostructured, ultrafine fullerene particles

Abstract

Aerosol synthesis methods for production of nanostructured fullerene particles have been developed. The nanostructured, ultrafine fullerene particles were produced in continuous flow reactor systems.

The study demonstrated that ultrafine (30–60 nm) fullerene particles can be generated by vapor condensation. The particles are spherical, solid and polycrystalline at processing temperatures of 500 °C and above. The larger fullerene particles with sizes around 100 nm were produced via an aerosol droplet drying and crystallization method. The particles are mainly nanocrystalline at processing temperatures of 20–200 °C and polycrystalline at 300–400 °C. At 500–600 °C the fullerene particles are mainly single crystals and sometimes clearly faceted.

The most common shapes among perfectly faceted particles were hexagonal plate-like, decahedral and icosahedral. The plate-like particles are lamellar twinned and the decahedral and icosahedral particles are multiply twinned. The lamellar-twinned particles probably grow rapidly on the side-faces in the direction parallel to the twins by a re-entrant corner growth mechanism. No uniform mechanism was found for the formation of multiply-twinned particles. They probably grow layer-by-layer around the exiting decahedral and icosahedral nuclei or are formed during grain growth from polycrystalline particles. The growth of particles with well-defined crystal habits is often promoted by defects, such as twins and stacking faults. The vaporization of fullerene particles in the heated zone of the reactor plays an important role during the formation and growth of particles with a clearly faceted shape.

The study shows that fullerene particles with controlled size and crystallinity can be produced by aerosol synthesis methods.

Keywords
aerosols, synthesis, nanostructured materials, particles, fullerenes, vapor condensation, droplet drying, crystallization, transmission electron microscopy, morphology

Activity unit
VTT Chemical Technology, Process Technology,
Biologinkuja 7, P.O.Box 1401, FIN–02044 VTT, Finland

ISBN	Project number
951–38–5545–7 (soft back ed.) 951–38–5548–1 (URL: http://www.inf.vtt.fi/pdf/)	KETT94152

Date	Language	Pages	Price
November 1999	English	64 p. + app. 101 p.	D

Commissioned by
Technology Development Center (Tekes); VTT Chemical Technology; Ventipress Ltd.;
European Science Foundation (ESF)

Series title and ISSN	Sold by
VTT Publications 1235–0621 (soft back ed.) 1455–0849 (URL: http://www.inf.vtt.fi/pdf/)	VTT Information Service P.O.Box 2000, FIN–02044 VTT, Finland Phone internat. +358 9 456 4404 Fax +358 9 456 4374